ACS OMEGA

http://pubs.acs.org/journal/acsodf

Review

Ordered Mesoporous Electrodes for Sensing Applications

María L. Scala-Benuzzi, Sol N. Fernández, Gustavo Giménez, Gabriel Ybarra, and Galo J. A. A. Soler-Illia*

Cite This: *ACS Omega* 2023, 8, 24128−24152

Read Online

ACCESS | Metrics & More | Article Recommendations

ABSTRACT: Electrochemical sensors have become increasingly relevant in fields such as medicine, environmental monitoring, and industrial process control. Selectivity, specificity, sensitivity, signal reproducibility, and robustness are among the most important challenges for their development, especially when the target compound is present in low concentrations or in complex analytical matrices. In this context, electrode modification with Mesoporous Thin Films (MTFs) has aroused great interest in the past years. MTFs present high surface area, uniform pore distribution, and tunable pore size. Furthermore, they offer a wide variety of electrochemical signal modulation possibilities through molecular sieving, electrostatic or steric exclusion, and preconcentration effects which are due to mesopore confinement and surface functionalization. In order to fully exploit these advantages, it is central to develop reproducible routes for sensitive, selective, and robust MTF-modified electrodes. In addition, it is necessary to understand the complex mass and charge transport processes that take place through the film (particularly in the mesopores, pore surfaces, and interfaces) and on the electrode in order to design future intelligent and adaptive sensors. We present here an overview of MTFs applied to electrochemical sensing, in which we address their fabrication methods and the transport processes that are critical to the electrode response. We also summarize the current applications in biosensing and electroanalysis, as well as the challenges and opportunities brought by integrating MTF synthesis with electrode microfabrication, which is critical when moving from laboratory work to *in situ* sensing in the field of interest.

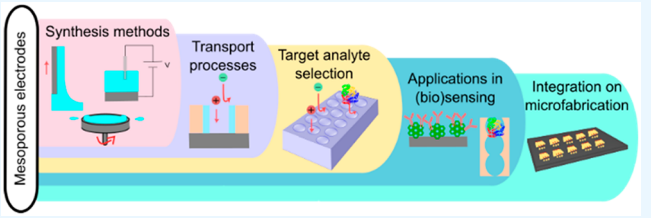

1. INTRODUCTION

Mesoporous materials have attracted widespread interest in the last two decades due to the possibility of building complex nanoarchitectures with very high structural control in a few and relatively simple synthetic steps. The combination of chemical synthesis and supramolecular templating leads to spatially organized arrays of mesopores (i.e., 2−50 nm in diameter). Functionalization of the inorganic walls, mesopore surfaces, or pore volume with molecular, biomolecular, or nanostructured functions leads to multifunctional matrices with large available surface area and tailorable interfacial properties, leading to applications in several fields: biomedical, analytical, or energy.[1−7]

In addition to these features, new phenomena due to the limited mesopore size such as selective adsorption, solvent confinement, or molecular partition arise that can be exploited in novel applications. Moreover, control of the intricate architectural regions (pore wall, pore surface, and pore interior) permits tailoring of several relevant properties such as pore accessibility, surface reactivity, and the distance and/or intimate contact between molecular or nanostructural functions. Mesoporous nanoarchitectures can be indeed used as localized intercommunicated nanoreactors, constituting therefore a playground for the creative development of novel chemical nanosystems that combine nanofluidics and confined sorption and reactivity processes.[8]

These innovative materials can be processed as Mesoporous Thin Films (MTFs) that display controllable thickness, highly organized, and tunable pore systems as well as a versatile framework composition. Ideally, these systems should present high chemical and mechanical stability in order to be applied in optical, optoelectronic, or electrochemical devices.[6,9−12] Since the first reports on mesoporous thin films through surfactant-templated synthesis,[13−15] the field has emerged and their use and applications have been widely extended to solar cells,[16,17] batteries and supercapacitors for energy storage,[18,19] photocatalysis,[20] separation and/or adsorption membranes,[21] photochromic devices,[22] photonics,[23] sensors,[24] and biosensors,[25] among others.

In the field of electrode modification, nanomaterials have become one of the main means of producing electrodes with improved performance. Several works have confirmed the

Received: March 25, 2023
Accepted: June 9, 2023
Published: June 29, 2023

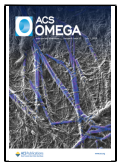

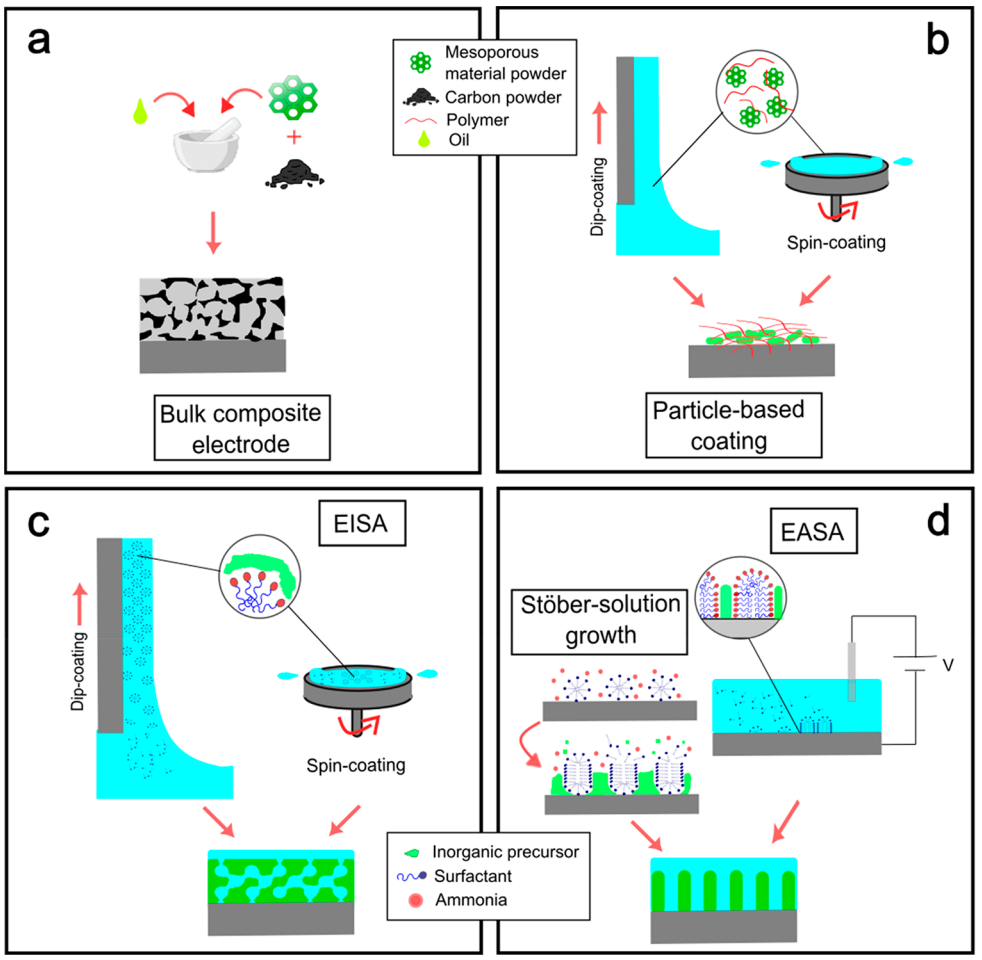

Figure 1. Schematic representation of the methods of mesoporous electrode fabrication. (a) Bulk composite electrode. (b) Particle-based coating. (c) Evaporation Induced Self-Assembly (EISA). (d) Electro-Assisted Self-Assembly (EASA).

benefits of nanostructured electrodes in sensors and biosensors due to their increased surface area and size-dependent electronic structure.[26] Mesoporous thin films offer the possibility of a precise tailoring of their inorganic walls, high surface area, controlled pore size, and surface functionalization,[6,12,27−29] which are particularly interesting for the design and construction of electrodes. These features enable unique sensing potentials based on the precise control of interfacial processes (adsorption and electron transfer), nanofluidics, and molecular sieving (size or charge exclusion). MTF-modified electrodes present several desirable features, such as reproducible preparation, robustness, and straightforward integration to electroactive substrates (metals, carbon, and conductive inorganic solids). Additionally, MTFs are usually transparent, allowing the coupling of optical signals to electrochemical processes. Furthermore, depending on the composition of the film, the framework walls can offer improved (electro)catalytic or optoelectronic properties.[30,31]

In the present review, we present an overview of MTF-based electrodes, and we discuss their sensing applications from an integral approach that considers the points of view of the communities belonging to materials and physical and analytical chemistries. First, a brief description of the pathways leading to mesoporous thin films is presented, highlighting the methods to obtain mesoporous electrodes. In particular, we focus this work on an in-depth comparison between the two most used MTF synthesis routes: Evaporation Induced Self-Assembly (EISA) and Electro-Assisted Self-Assembly (EASA). Both methods permit obtainment of homogeneous thin films with excellent substrate adhesion that leads to chemically and mechanically robust modified electrodes. We discuss in detail the structural and chemical features of MTFs obtained by both methods.

Second, an in-depth discussion of the transport processes inside the mesoporous thin films is presented. At this stage of development of the field, it is necessary to analyze the complexity of the mass and charge transport phenomena that take place in these electrodes under confinement. Several studies are described and discussed that relate the electrochemical response to the mesostructure and pore diameter. Furthermore, this is related to the electrode accessibility and the analyte selection and concentration by the mesoporous thin film.[32−34] Finally, some current applications of these platforms in biosensing are presented and discussed as well as the integration of MTF-modified electrodes in sensors combined with classical silicon-based microelectronics.

2. PRODUCTION OF ELECTRODES MODIFIED WITH TEMPLATED MESOPOROUS MATERIALS

For sensing applications, electrode surfaces are commonly modified with nanomaterials with the goal of improving the analytical figures of merit, stability, and robustness. In this context, mesoporous materials have been extensively used for electrode modification due to their unique structural properties

https://doi.org/10.1021/acsomega.3c02013
ACS Omega 2023, 8, 24128−24152

(controlled porosity, high surface area, and versatile functionalization, among others) that lead to excellent analyte transport capacity and high adsorption, which can be advantageously used in electrochemical sensing in order to achieve molecular sieving or preconcentration to reach higher selectivity and sensitivity. In addition, their adjustable framework and surface composition allow obtainment of a wide variety of electrode coatings from insulating materials to excellent conductors as required by the sensor application. It is important to clarify that this review will present and discuss MTFs made up through supramolecular templating processes that lead to organized mesopore arrays with typical diameters between 5 and 20 nm. Other techniques to produce porous thin films such as nanoporous alumina or porous silicon obtained by anodization or macro-mesoporous films obtained by colloidal assembly are out of the scope of this work.

2.1. General Methods to Obtain Mesoporous Electrodes. In general, two main configurations of mesoporous electrodes can be identified: the so-called "bulk composite" films and thin-film-coated electrodes.[35]

A composite electrode consists of at least one conductor phase and at least one insulator phase intermixed (Figure 1a).[36] Mostly, the conductive phase is a type of carbon powder, and the insulator one is a viscous liquid. Composite electrodes can be classified according to the way the component materials are distributed; both types of electrodes have features that can be exploited. Modified nanocomposite electrodes present some attractive features: they are easy to fabricate by simply mixing the components; they are highly versatile, which allows incorporation of any type of solid into the composite matrix; in addition, selectivity or sensitivity enhancers can be added straightforwardly into the bulk material.[37] The incorporation of mesoporous materials into composite electrode matrices can improve the specific surface area and specific capacitance.[38] These properties make bulk composite electrodes modified with mesoporous materials widely applicable in batteries and supercapacitors.[39]

Among film-coated electrodes, two different cases must be distinguished.[35] First, the formation of particle-based coatings onto the electrode (Figure 1b). These are formed by the dispersion of a mesoporous material powder, followed by deposition on the electrode (generally by dip- or spin-coating) and solvent evaporation. This simple method has, however, some critical disadvantages such as the lack of mechanical stability; furthermore, the materials present low conductivity.[40] In an effort to correct these drawbacks, the addition of several polymers in the mesoporous dispersion and/or the modification with metal nanoparticles[40] or carbon-based materials[41] have been reported.

Second, we can consider the generation of continuous and uniform thin films over the electrode. This kind of coating has the advantages of being synthesized in a one-step route, being able to be obtained with excellent homogeneity along with a large area, and presenting a uniform and controllable thickness, from pore monolayers to micro-thick, crack-free continuous films.[42] In order to obtain these modified electrodes, thin films have been prepared by dispensing the sol solution on the support material, by dip-coating or spin-coating, through the so-called "Evaporation-Induced Self-Assembly" (EISA) method.[9,15,43] EISA allows a high control of mesostructure type, pore size, and interconnectivity.[44] Other methods, such as the Stöber-solution growth approach[45] and the "Electro-Assisted Self-Assembly" (EASA),[46] allow obtainment of oriented pores perpendicular to the substrate, which is in principle a desired feature to optimize analyte transport. In particular, the use of EASA has spread rapidly in the past few years for the development of electrochemical sensors with vertically oriented channels. The EISA and EASA methods are simple and reproducible and lead to homogeneous and crack-free thin films with excellent substrate adhesion. Because of these characteristics, we propose an in-depth study of these two methods. Table 1 shows a comparison of the main characteristics and limitations of EISA and EISA, which will be analyzed in-depth in the following sections.

The choice of the synthetic method is essential in order to control crucial macroscopic features of the mesoporous films, such as hardness and residual stress (that can lead to adhesion failure and cracking) and wettability, among others,[47] in order to develop reproducible and eventually scalable preparation methods.[48]

The EISA and EASA synthetic methodologies have been discussed in-depth in several reviews, to which the interested reader is redirected.[6,12,28,29,69,70] However, we can summarize some common features that lead to MTFs with highly organized pore arrays. Both EISA and EASA are based on the spontaneous assembly (*self-assembly*) of the inorganic species and the template counterparts (*co-assembly*). An adequate control of the assembly and postsynthesis electrode processing are essential to achieve robust electrodes with open mesoporosity and stability under operation. In addition, both methods permit a straightforward integration in current electronics and optics sensor device production pathways. Essentially, both pathways rely on the controlled assembly of two different nanobuilding blocks (NBBs): the precursors of the material framework and the supramolecular template. In order to achieve control, thermodynamic and kinetic aspects of NBB morphology, production, and interactions should be taken into account.

In the case of EISA, solvent evaporation after coating leads to a mixture of the inorganic and organic NBBs in a concentrated, viscous gel that evolves toward mesostructuring.[49] Two competing processes take place: stiffening of the forming film versus mesoscale organization. A "race towards order" begins, which must be controlled to obtain an organized mesophase, as demonstrated by *in situ* measurements,[28,71,72] supported by theoretical development.[51,73] This approach permits a flexible choice of supramolecular templates and inorganic frameworks. In addition, postsynthetic treatment of the freshly formed mesostructured films permits regulation of order or annealing of the structure.[74,75] In the case of EASA, an adequate potential applied to a conductive electrode immersed into a silica acidic precursor sol promotes an increase of pH at the electrode surface that leads to Si-O-Si condensation. This potential also favors the assembly of a surfactant templating layer formed by hemimicelles adsorbed at the surface that assists in the controlled growth of vertically aligned mesoporous channels. This method has some limitations regarding the template molecule (alkylammonium bromides) that lead to limited size mesopores, although pore expanding agents can be used.[76] In this case, the NBBs are negatively charged Si-oxo clusters formed at pH (9−10) that interact with the positively charged alkylammonium templates and then condense to form the inorganic walls. In this sense, this synthetic route can be compared with the formation of MCM-41 through heterogeneous precipitation, which is triggered at the electrode interface through local alkalinization.

https://doi.org/10.1021/acsomega.3c02013
ACS Omega 2023, 8, 24128−24152

Table 1. Comparison of the Most Relevant Characteristics between the EISA and EASA Methods for Mesoporous Thin Film Production

	EISA	EASA
Driving force	Thermodynamic design of mesostructure,[49,50] kinetic control of co-assembly.[51]	A suitable cathodic potential provokes local pH changes which promote condensation.[46]
Substrate limitations	Any shape for dip-coating, only flat surface can be coated using spin-coating. No limitation of the substrate material is reported.	Any shape can be coated. Only conductive substrates. Limitation with Au substrates due to Br-containing surfactants (adhesion problem).[32]
Coatinglimitations	The process ensures total substrate coverage by the film. Minimum amount of sol is required for spin process. Thick and/or multilayered films are allowed.[52]	Thick and/or multilayered films are allowed.[53] Long deposition times generate aggregates on the film surface.[54,55]
Patterning techniques	Designed patterns are achieved by lift-off, soft patterning, or etching process.[56]	Patterns can be achieved by a deposition of metal previous to the MTF formation.
Surfactant template	Cationic surfactants; e.g. cetyltrimethylammonium bromide (CTAB). Nonionic surfactants (e.g., Brij 58, Brij 56), block copolymers (e.g., Pluronics P123 and F127).	Cationic surfactants, mostly CTAB, and other cationic surfactants with the form $[Me_3NC_nH_{2n+1}]Br$ (alkyl chain lengths between C14 and C24).[57]
Inorganic frameworks	Variety of oxides (Si, Ti,[58] Zr,[59] Ce, Mg, Ta, Co,[60,61] W,[62] Mo,[63] Nb[64]). Carbon,[65] phosphates.[66] Mixed oxides[67] or NP-derived materials can also be obtained.	Only SiO_2 reported, with possible extension to another metal centers.
Pore structures	2D (Lam = lamellar, *p6m*, and *c2 mm*), 3D (R3m, *I4/mmm*, Fm3m, Im3m, $P6_3/mmc$, and Pm3n), and bicontinuous (Ia3d and Pn33m).[68]	Hexagonally packed 1D channels that grow normal to the electrode surface.[46]
Functionalization	Pre- and postfunctionalizations are reported.[47]	Postfunctionalization has been reported.[6]

In both synthetic routes, the expected features (i.e., wall composition, pore volume, diameter, spatial arrangement and interconnectivity, surface charges, or chemical dangling groups) can be controlled in principle by external parameters and materials processing, as we briefly discuss below. In order to understand the relevant material features, the mesoporous film/electrode systems must be thoroughly characterized through structural and textural techniques. As mesoporous films are quite a complex nanosystem, a variety of structural, spectroscopic, and imaging techniques should be used to afford a complete characterization of the final devices. We refer to work that covers in detail this central aspect,[58,69,77] including the mechanical properties, which are essential for electrode performance.[78]

2.2. The Choice of the Inorganic Precursors. The inorganic species that form the pore walls are typically produced through sol−gel chemistry routes that consist of controlled polymerization of alkoxide or chloride precursors under mild temperature conditions. Typically, metal centers are activated and then linked with oxo or hydroxo bridges, generating metal-oxo or metal-hydroxo polymers in solution. This is carried out in two steps: hydrolysis and condensation.[79,80]

An adequate handling of the chemical variables involved in hydrolysis and condensation leads to control of the final properties of the sols used as film precursors. A critical aspect is the condensation degree, the size, and the philicity of the inorganic species, which are determinants in order to optimize the self-assembly with the supramolecular templates. For example, the hydrophobic/hydrophilic characteristics will determine interactions with the organic template, which in turn will be essential for controlling the mesopore structure.[81,82] Recent theoretical and experimental studies have shown that the radius of gyration of the inorganic species is crucial in order to obtain a well-defined mesostructure in EISA, opening the pathway to create highly ordered mesoporous films using preformed inorganic nanobuilding blocks.[83,84]

On the other hand, the composition and structure of the precursor inorganic species determine the type of inorganic material that will be obtained. The most extended mesoporous material in thin films is silica. A large variety of non-siliceous oxide MTFs are oxides such as high-valence transition metal oxides such as TiO_2, WO_3, Nb_2O_5, SnO_2, MnO_2, and CeO_2; some recent works have reported low-valence Al_2O_3[85] and ZnO[86,87] or nanoparticle-based Ni- or Co-based oxides.[88,89] Non-silica matrices are particularly interesting due to the modulation of electronic and optical properties, in addition to their increased chemical stability, the exploitation of charge transfer processes, and also their intrinsic catalytic activities.[10,90]

Furthermore, inorganic−organic hybrid MTFs (MHTFs) can be obtained through one-pot or postgrafting synthesis. In the case of one-pot strategies, typically organically modified alkoxides (OMAs) are added as precursors, which are available in a great variety. Control of the OMA reaction with transition metal alkoxides or metal salts can lead to hybrid materials with intimately mixed metal centers, presenting an enormous variety of compositions.[28,91]

2.3. Postprocessing and Template Removal. Once the mesostructure has been attained, template removal permits the acquisition of accessible mesopores. This is a crucial step because structural consolidation of the inorganic walls along

https://doi.org/10.1021/acsomega.3c02013
ACS Omega 2023, 8, 24128−24152

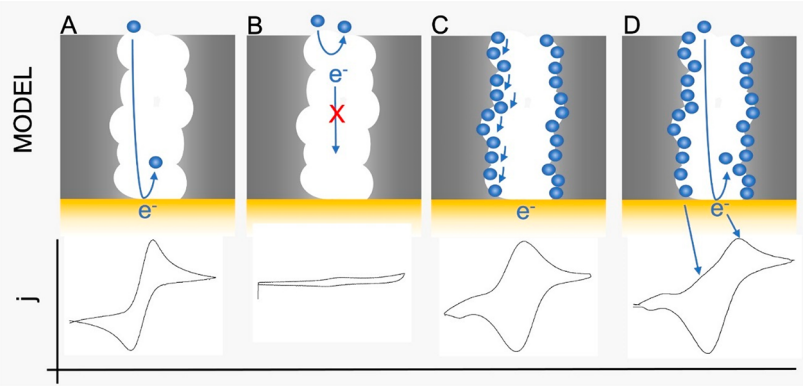

Figure 2. Schematic representation of the most usual transport mechanisms of electroactive molecules along a mesoporous layer deposited onto an electrode. (A) Diffusion. (B). Exclusion (electrostatic or steric). (C) Adsorption followed by charge hopping. (D) A combination of hopping and diffusion. Typical cyclic voltammograms (j vs E) are depicted below each case.

template removal might change the pore features or may lead to cracking.[92] Commonly, in EISA synthesis, thermal treatment at 130 °C is carried out after deposition to stabilize the inorganic framework, followed by a high-temperature treatment, between 350 and 600 °C, depending on the authors, to further consolidate the film and remove the organic template by calcination. This treatment generates a uniaxial contraction along the film thickness that generally leads to changes in pores and neck diameters; generally, higher temperatures lead to wider necks and smaller pores due to partial sintering.[93] High-temperature treatment also leads often to crystallization, which in the case of non-silica oxides increases MTF conductivity and photoactivity.[93−95] Particular attention has to be paid to electroactive substrates that can affect crystallite growth, pore evolution, and catalytic performance.[96] The use of bulky templates combined with stabilization processes under an inert atmosphere at intermediate temperatures leads to the formation of a carbonaceous scaffold that permits avoidance of large uniaxial film contraction and therefore retains larger mesopores.[97]

A central limitation of thermal surfactant removal is that it cannot be used for MTFs deposited onto thermally labile substrates such as polymers. For this reason, other removal routes have been proposed as alternatives to calcination. For example, Giménez et al. presented consolidation−extraction methods by refluxing EISA-derived silica MTFs in different solvents or exposed to vacuum. Low-temperature postsynthetic treatment methods allow silica condensation and improve phase separation of the template, leading to robust silica frameworks with well-defined, accessible mesopore systems.[98]

Walcarius and co-workers proposed an overnight treatment for EASA-derived MTFs at 130 °C followed by a template removal step carried out by in ethanol solution containing 0.1 M HCl under moderate stirring for 5 min.[46] Cyclic voltammetry experiments were performed before and after the extraction in order to verify the template removal. Despite the simplicity of this extraction method, the percentage of effective removal has not been reported in detail.

3. TRANSPORT PROCESSES INSIDE MTF-COATED ELECTRODES

In the case of electrochemical sensors, electrode modification is performed using either isolating (silica) or semicrystalline (titania, zirconia, mixed oxides) MTFs with low conductivity. Therefore, the origin of the faradaic current is mostly due to the redox processes that take place at the electrode surface. Extended nanocrystalline walls lead to faradaic reactions also taking place at MTF surfaces, which are of use in energy or catalysis-related applications such as batteries, supercapacitors, or photoelectrodes.[19] But in the case of sensors, the MTF layer is generally used as a perm-selective layer, which is intended to modulate molecule transport, exclusion, or preconcentration. In principle, MTFs can be advantageously tailored in order to control molecular transport toward and from the electrode. Among the most relevant controllable MTF features, we can cite the framework composition, surface chemistry, pore size, mesostructure, and interconnectivity. These factors can indeed affect the movement and spatial distribution of species confined inside the mesopores. In turn, these factors clearly influence the mass and charge transport toward and from the electrode. In the past few years, these complex processes have been explored by several techniques, in particular cyclic voltammetry[99] or fluorescence.[100] A scheme of the basic molecular transport in mesopores is presented in Figure 2, along with the typical cyclic voltammetry signals recorded for electrochemical probes diffusing along the mesoporous layer, which are central to the development of electrochemical sensors. It is worth mentioning that analytical signals in most of the mesoporous-based sensors are the result of the selective passage of an electroactive analyte, which is detected as a faradaic current resulting from the electron transfer reaction at the electrode surface. Voltammetric techniques are the most adequate to analyze these kinds of phenomena because voltammograms can be easily and speedily obtained and interpreted. Cyclic voltammograms provide a fast means of obtaining information related to the nature of the diffusion process through the shape of the peak and peak potential, as well as information related to the concentration of the analyte through the the peak current (Figure 2). On the other hand, other voltammetric techniques such as square wave voltammetry (SWV) and differential pulse voltammetry (DPV) can be more adequate toward analytical ends, since they allow researchers to reach higher sensitivity and lower limits of detection (LODs), with improved peak resolution.

Most transport studies have been carried out for template-free MTFs, which present an electrochemical response greatly modulated by the interactions between the channel walls and the redox probe. The most ideal situation is the diffusion of a free probe across the mesopores (Figure 2A). This behavior leads to electrode currents that roughly display a cyclic

https://doi.org/10.1021/acsomega.3c02013
ACS Omega 2023, 8, 24128−24152

voltammetry (CV) behavior that can be analyzed following the usual diffusion analysis (see below for a more accurate discussion). Some applications that take advantage of the hydrophobic nature of template-loaded channels are described in section 4.1.2.

Since the first works, it was clear that the interactions of the electroactive probe with the mesopore walls can lead to permselective behavior, therefore modifying its diffusion, leading to preconcentration or even exclusion.[101] These behaviors can be advantageously used either to preconcentrate an analyte or to exclude an interference. In the following sections, we discuss these aspects in detail.

Changes in diffusion due to electrostatics. When an MTF is immersed in a solution, a net charge can develop on the mesopore surface. The charge fixed on the pore surface can attract oppositely charged species or lead to the exclusion of similarly charged ones. In the most typical case of mesoporous oxides, the magnitude of the surface charge depends on the material, the pH of the solution, and the isoelectric point (IEP) of the oxide, which is a consequence of the acid/base equilibria of surface groups (e.g., silanol/silanolate). In the case of silica, the IEP is approximately 2; therefore, silica presents a negative surface charge under most usual working conditions. Another factor affecting the magnitude of the surface charge is the number of possible ionizable sites per surface unit, which in the case of silica is ca. 4.6−4.9 silanol groups per nm^2.[102] In the case of titania, the empirically reported IEP shows a broad range, mainly due to surface defects. Table 2 shows the IEP of some of the most common MTFs used.

Table 2. Isoelectric Point for Some Materials Used in MTF

Material	IEP range or approx.
Silica[103]	2
Titania[104]	2−8.9
Zirconia[105]	5.5−9.5

The electric field generated by the surface charge combined with the mesoporous structure geometric factors is an important component of MTF permselective behavior. In order to evaluate the relevance of the electrostatic effect, it is useful to compare the electric field within the mesopore to the actual pore diameter. The electrical potential in the pore decays from the value of the zeta potential at the wall surface to its minimum at the pore center. This potential is modulated by the double layer thickness, or Debye length (λ_D), which can be calculated according to eq 1:

$$\lambda_D = \sqrt{\frac{\epsilon_0 \epsilon_r k_B T}{2 N_A e^2 I}} \quad (1)$$

where ϵ_0 is the permittivity of free space, ϵ_r is the permittivity of water, k_B is the Boltzmann constant, T is the temperature, N_A is the Avogadro number, e is the elementary charge, and I the ionic strength.

The potential distribution inside the pores is a function of the *zeta*-potential, and the Debye length gives an idea of the spatial potential decay, which depends on the concentration of ionic species in the mesochannel. Since the electric field vanishes from the wall, the ratio between the channel size and λ_D defines whether the ionic layers overlap inside the pores. Characteristic values of λ_D for a 1:1 electrolyte in water span from approximately 0.3 nm (1 M) to 1 nm (100 mM) to 10 nm (1 mM).[106] Thus, for ionic strengths higher than 50 mM, λ_D is shorter than the mesopore diameter and thus ionic layers do not overlap. The central zone of the channels presents a constant and low potential where ions can move more freely. For instance, in the case of vertically aligned channels, the channels are divided into two zones for $r > \lambda_D$, where r is the channel radius. One of them consists of a Debye layer in contact with the pore wall (where there is a potential gradient), and the other one corresponds to "free" space (constant potential) in the center of the mesochannel. As the ionic strength decreases, the Debye layer increases, so the "free" space is reduced, until it disappears completely when $r < \lambda_D$, leading to an overlap of the double layers.

In the case of MTFs presenting pores and necks, the smaller diameter of the necks can lead to enhanced permselectivity due to the overlap of ionic layers. This behavior was corroborated by fluorescence correlation spectroscopy studies that demonstrated the existence of two transport regimes in low- and high-ionic-strength media.[107] In low-ionic-strength conditions, a Fickian diffusion was found for Rhodamine B molecules used as optical probes; measured diffusion coefficients were 2 or 3 orders of magnitude lower compared to the free probe in water and practically independent of mesopore or neck size. This can be attributed to a high electrostatic attraction between the probe and walls of opposite charge that leads to probe adsorption onto the mesopore surface. On the contrary, at high ionic strength, the Debye layer is compact, and diffusion is modulated by the pore and neck diameter. In these conditions, diffusion values slightly increase with increasing diameters, reaching a practically constant value for a neck radius >2.8 nm. These findings demonstrate the relevance of molecule−wall interactions on mobility and the relevant role of the Debye layer in the confined transport of charged probe species.

The voltammetric response of partially or totally excluded redox species in mesoporous oxide thin films can be therefore explained in terms of the strong electrostatic repulsion between the similarly charged surface and the redox species (Figure 2A), taking into consideration the ratio between λ_D and mesopore diameter. When the surface charge is low or highly screened, the electrostatic permselective effects are slight, and voltammograms with the usual semi-infinite diffusion conditions have been reported, attenuated by geometrical restrictions such as interpore necks, that can be generally interpreted as a tortuosity factor.

In cases where the surface charge and the redox species have opposite charge, the redox species can be adsorbed due to a strong electrostatic interaction. From the analytical point of view, this leads to preconcentration and can lead to an increase in the electrochemical signal. If the concentration of adsorbed redox species in the film is high enough, redox sites can be close enough so that electron hopping between them is feasible (Figure 2C). The electrochemical signal due to the adsorbed redox species is often combined with the signal due to free species; the resulting voltammogram resembles those of thin electrochemical cells (i.e., complete reduction and oxidation of bonded and interconnected redox species inside the MTF), as illustrated in Figure 2D. The existence of adsorbed and free species is reflected in a theoretical model.[108]

Surface charges can also be incorporated into MTFs by including charged groups by prefunctionalization, postfunctionalization, or grafting. Organosilanes are particularly suited to this purpose since they permit a straightforward and widespread chemistry for surface modification. Surface amino

https://doi.org/10.1021/acsomega.3c02013
ACS Omega 2023, 8, 24128−24152

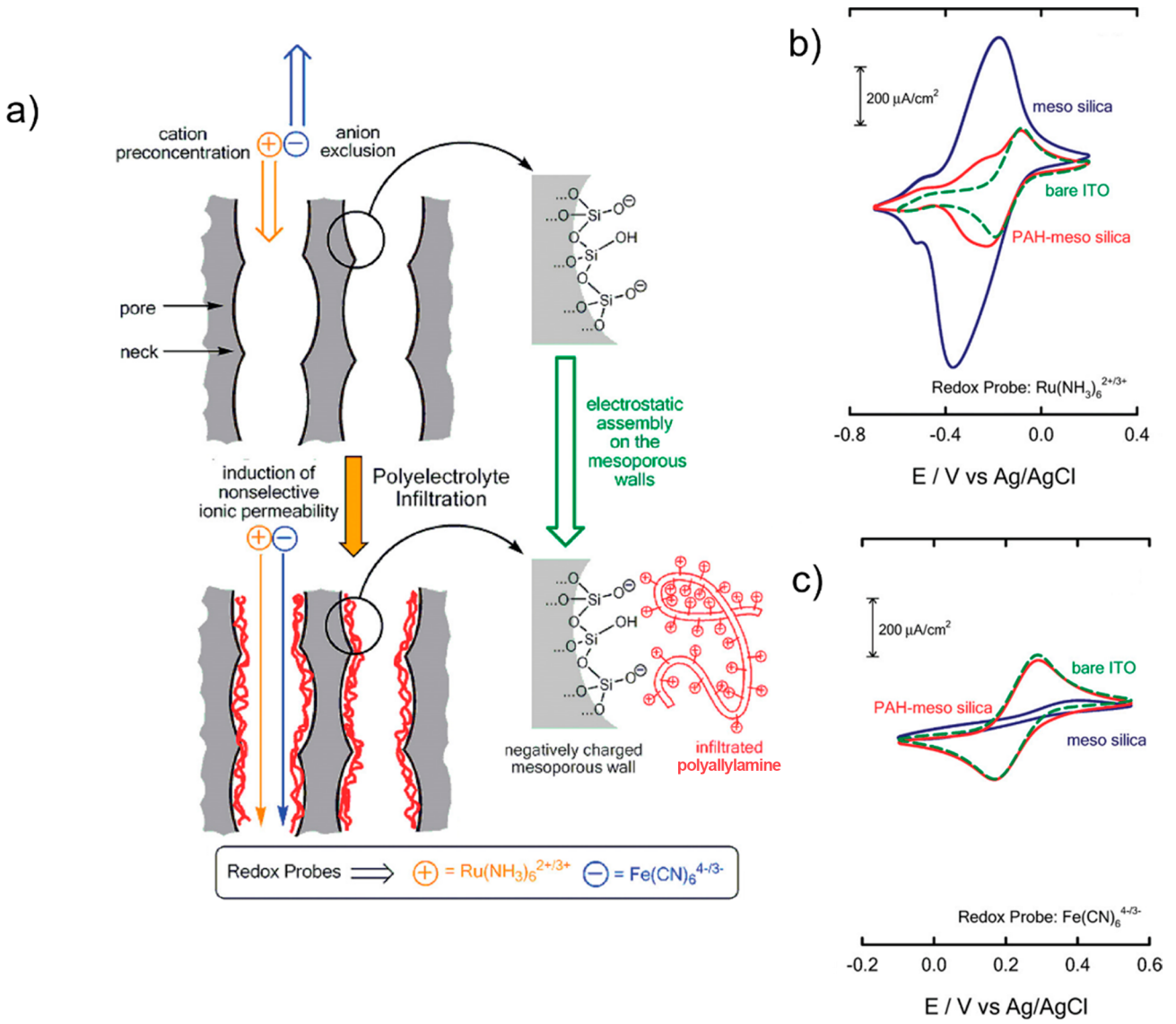

Figure 3. (a) Scheme of the infiltration of polyallylamine inside the mesoporous silica film. Cyclic voltammetric studies used (b) $Ru(NH_3)_6^{3+}$ as a cationic redox probe and (c) $Fe(CN)_6^{3-}$ as an anionic redox probe. The different traces correspond to (blue trace) a bare mesoporous silica film, (red trace) a PAH-infiltrated mesoporous silica film, and (dashed green trace) a bare ITO substrate. Scan rate: 200 mV/s. Electrolyte: 1 mM redox probe + 0.1 M KCl (pH 5). Reprinted with permission from Brunsen et al. *Langmuir* **2011**, *27*, 4328−4333. Copyright 2011 American Chemical Society, ref 110.

modification performed using 3-aminopropyltriethoxysilane (APTES) leads to noteworthy changes in probe exclusion and transport, linked to the changes in IEP of the modified silica, as demonstrated by combining the CV results with XPS and simulation experiments.[91,109] Surface modifications can also be performed by polyelectrolyte adsorption. Brunsen et al.[110] proposed the direct infiltration of a polyelectrolyte in the mesoporous framework to control the ion transport through the film (Figure 3).

Steric exclusion. In addition to surface charge, steric and philicity aspects must be considered in the transport within the pores. Otal et al. demonstrated that diffusion through titania MTF electrodes was modified after surface functionalization with organic modifiers.[32] This pore-blocking effect depends on two factors related to the functionality excluded volume (i.e., the combination of actual function volume and surface grafting density) and polarity. In principle, molecule transport can be regulated by playing with the functions of volume and polarity. In an extreme case, hydrophobic modifiers with long alkyl chains completely block ionic probe diffusion, but uncharged probes can diffuse through the pores. In the case of bulky organic functionalizers, the transit of the charged probe is hindered due to the reduction of the cross-section of the pore or due to interpore neck blockage. However, this type of modifier does not completely block the diffusion of uncharged probes; in some cases, indeed, a preconcentration may occur that enhances the signal.

As can be noted, several means of chemical and structural modifications and working conditions (pH and ionic strength) are available to modulate the mass and charge transport in MTFs, which can find application in electrochemical sensing. In particular, the use of polyelectrolytes helps tune the available surface charge, permitting charge reversal depending on the polyelectrolyte charge or chain length.[108,111]

3.1. Electrochemical Characterization by Cyclic Voltammetry. As discussed above, charge transport in

https://doi.org/10.1021/acsomega.3c02013
ACS Omega 2023, 8, 24128−24152

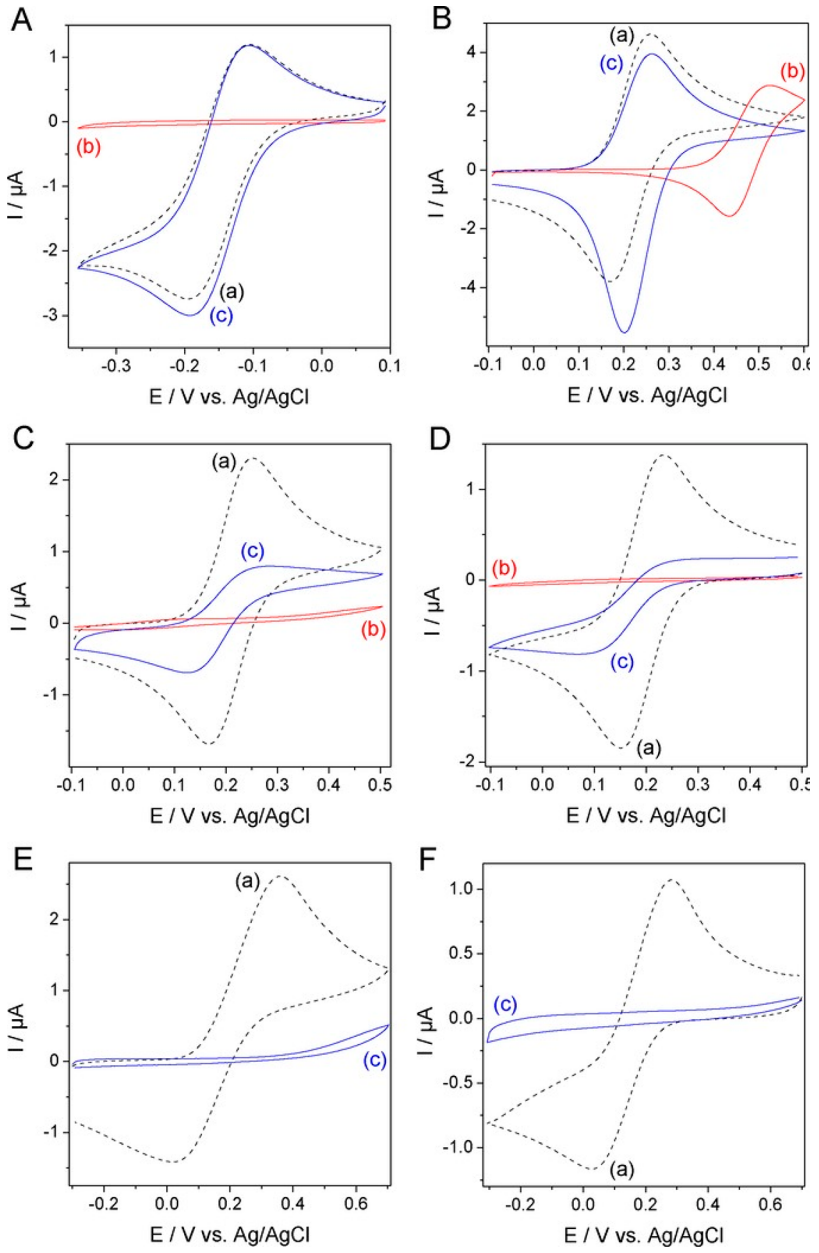

Figure 4. Cyclic voltammograms recorded in 0.1 mM solutions of (A) $Ru(NH_3)_6^{3+}$, (B) $Fc(MeOH)_2$, (C, E) $Fe(CN)_6^{4-}$, and (D, F) $Fe(CN)_6^{3-}$ by using (a, black) bare ITO and (b, c) ITO electrodes modified with vertically aligned mesoporous silica films before (b, red) and after (c, blue) surfactant extraction. Supporting electrolyte solutions were either 0.1 M $NaNO_3$ (A–D) or 1 mM $NaNO_3$ (E, F). Potential scan rate: 20 mV s^{-1}. Reprinted with permission from Karman et al. *ChemElectroChem* **2016**, *3*, 2130–2137. Copyright 2016, Wiley, ref 117.

MTFs takes place by the movement of electroactive species or by electron hopping between redox species. Cyclic voltammetry (CV) has been extensively used to assess the electrochemical response of MTF-coated electrodes. This technique provides a fast means of obtaining information about exclusion or preconcentration of ions, film integrity, and the characteristics of the film, which can affect mass and charge transport, such as pore blockage and channel tortuosity.

Depending on the degree of interaction of the redox probes with the channel walls, two main possible mechanisms of charge transport arise, as schematized in Figure 2: (i) physical diffusion of unbound redox species through the channels (weak probe–wall interaction, highly permeable films) and (ii) electron hopping between nearby bound redox species. These mechanisms can usually be elucidated by CV, since their voltammograms present a different shape, and they differ in the dependence of the peak current on the scan rate.

For a semi-infinite diffusion-controlled and electrochemically reversible electron transfer process on an uncoated electrode, the Randles–Ševčik equation describes the linear relationship between the peak current i_p (A) and the square root of the scan rate υ (V s^{-1}):

$$i_p = 2.69 \times 10^5 n^{3/2} A D^{1/2} \upsilon^{1/2} C \quad (2)$$

where n is the number of electrons involved in the redox process, A is the electrode area (cm^2), D is the diffusion coefficient (cm^2 s^{-1}), and C is the probe concentration (mol cm^{-3}).

Since the Randles–Ševčik equation is derived for a pristine electrode, it does not provide an adequate means of

https://doi.org/10.1021/acsomega.3c02013
ACS Omega 2023, 8, 24128–24152

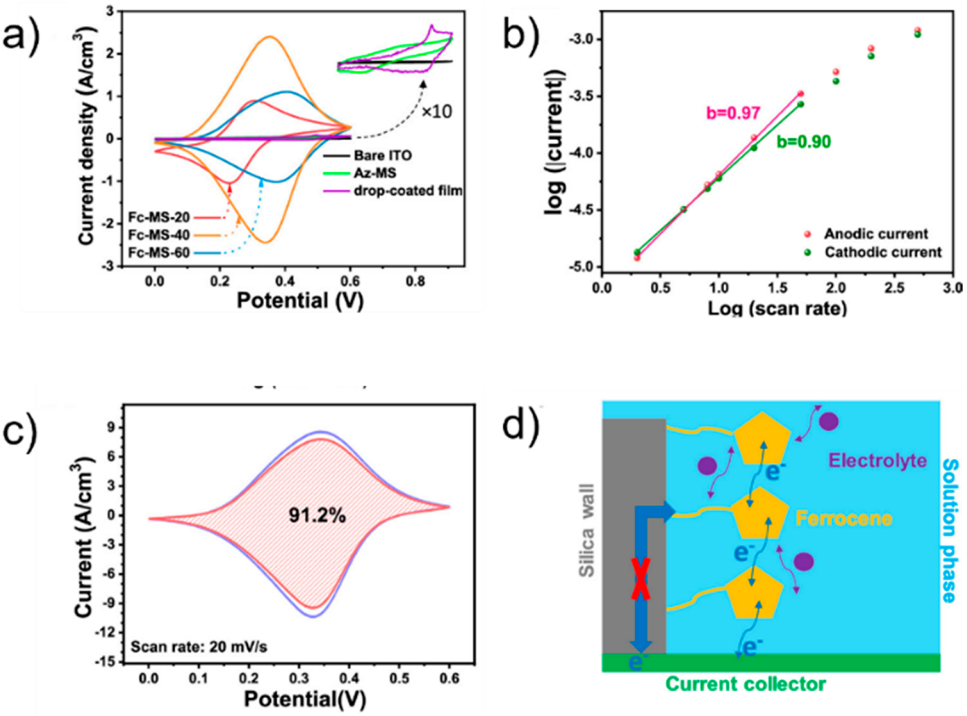

Figure 5. (a) Comparison of the CV curves recorded at 5 mV s^{-1} in 1 M LiCl using bare ITO and ITO ferrocene-functionalized film electrodes coated with Fc-MS-20, Fc-MS-40, Fc-MS-60, and Az-MS, and a ferrocene-functionalized film prepared from the drop-coating method. (b–d) Analysis of the redox process of Fc-MS-40. (b) Variation of the anodic and cathodic peak currents recorded by CV as a function of the potential scan rates (log scale). (c) Capacitive contribution of the oxidation process at the scan rate of 20 mV s^{-1} marked by the shaded region. (d) Illustration of the electron-hopping redox process taking place in the ferrocene-functionalized mesoporous silica film. Adapted with permission from J. Wang et al. *ACS Appl Mater Interfaces* **2020**, *12*, 24262−24270. Copyright 2020, American Chemical Society, ref 119.

interpretation for CV results with MTF-coated electrodes. Nevertheless, in some cases, it can be used to obtain simplified insight into the diffusion process of unbound electroactive species in MTFs. For instance, while studying the voltammetric results obtained for a titania hybrid MTF functionalized with organic molecules to be used as selective membranes, Otal et al.[32] observed linear i_p vs $v^{1/2}$ plots. Lower slopes were obtained for MHTF-coated electrodes with respect to those of the uncoated ones. Assuming a concentration inside the film equivalent to that of the bulk, a lower effective diffusion coefficient (D_{eff}) was calculated for the films, and this difference was attributed to the tortuosity (τ) introduced by the pore systems, which can also encompass the additional resistance to diffusion due to the presence of the organic molecules.

However, a constant value of concentration for the redox species cannot be assumed, in general. Interaction of redox species with the channel walls affects simultaneously the concentration of redox species inside the channels as well as the diffusion process itself, and consequently, an effective value of the product $D_{eff}^{1/2}C$ can be evaluated using the Randles−Ševčik equation from linear i_p vs $v^{1/2}$ plots, but not the individual values of the concentration inside the film (C_f) or the diffusion coefficient in the MTF (D_f). Finally, it is worth noting that the electrode area A in the Randles−Ševčik equation in MTF-coated electrodes is theoretically equivalent to that of an uncoated electrode. The MTF covers a fraction of the electrode area, and thus the electroactive area is reduced. However, the MTF-coated electrode can be considered as an array of nanometric ultramicroelectrodes separated by the walls of the channels. As discussed by Steinberg et al. (see section 3.1.2), the partial coverage of the electrode by the MTF does not result in a lower apparent value of A, since the hemisphericalrate. diffusion profiles of ultramicroelectrodes overlap and the final result is equivalent to that of a bare planar electrode.[112] Therefore, a more complete model is needed in order to describe the systems in a more quantitative way.

In addition, when the average distance between nearby redox probes is small, electron hopping between them becomes feasible. This occurs frequently in the MTF when there is a strong interaction between the electroactive species and the walls of the channel. A usual case is strong electrostatic interaction between oppositely charged redox species and ionized species from the wall, which promotes the buildup of redox species inside the MTF up to a grade in which eventually electron hopping can take place. Voltammograms in those cases usually present the typical symmetrical shape due to thin-layer cell conditions, where the current peak presents a linear dependence with the scan[113,114]

In conclusion, CV is useful to extract the general behavior of electroactive probes from current−voltage curves. Although many works dealing with sensing rely on a simplified Randles−Ševčik approach to deal with the concentration dependence of the obtained currents, care has to be taken in understanding the nature of the peaks in order to correctly separate the contributions of free and adsorbed species. There is still a need for more accurate models that can shed light on the complexities of confinement and exclusion effects, especially for multicomponent systems.

3.1.1. CV as a Tool for Assessing Accessibility, Template Extraction, and Integrity. Electroactive redox probes have also been used to assess the film integrity and electrode

https://doi.org/10.1021/acsomega.3c02013
ACS Omega 2023, 8, 24128−24152

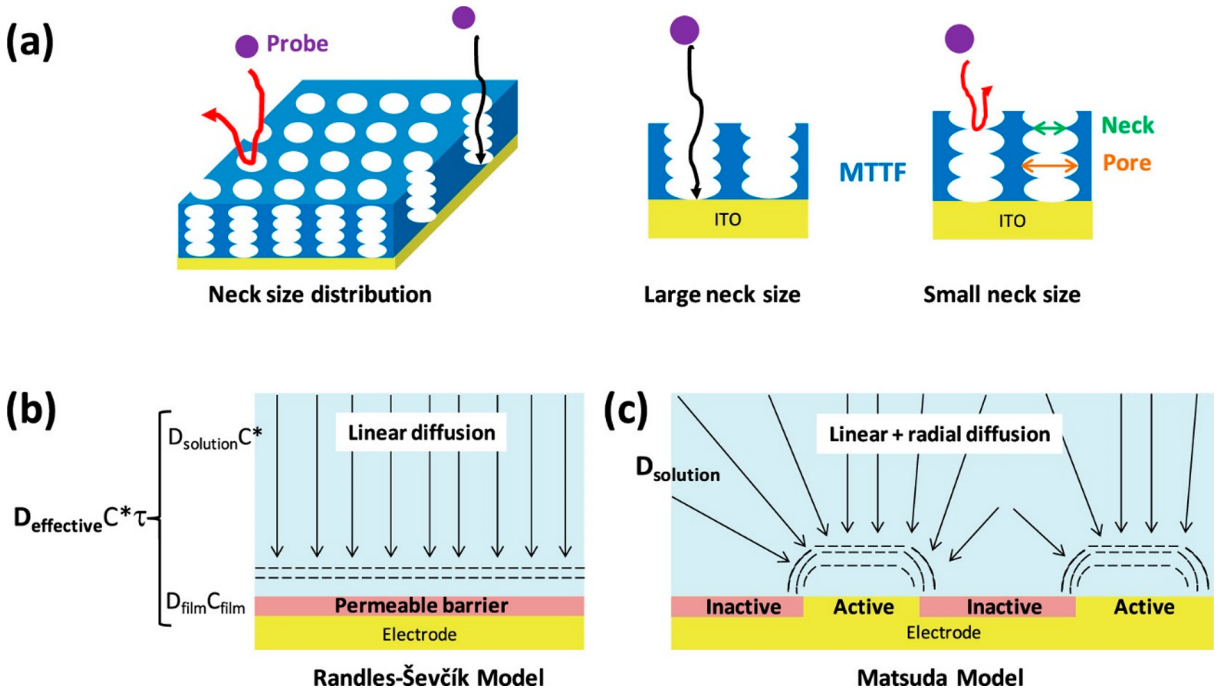

Figure 6. (a) Schematic representation of the surface-to-bottom connectivity for molecular probe transport through mesoporous films. Main features of the (b) Randles−Ševčik model and (c) Matsuda model.[128] Adapted with permission from P. Steinberg et al., *J. Phys. Chem. C* **2021**, *125*, 23521−23532. Copyright 2021, American Chemical Society, ref 112.

accessibility. For instance, hexacyanoferrate, a negative redox probe, can be employed to test the homogeneity and integrity of silica MTFs which are negatively charged at pH > 2. Figure 4 shows that different oxidation and reduction processes can be observed in the voltammograms depending on the probe used. Negatively charged ferro- or ferricyanides are excluded from the film. The absence of faradaic processes demonstrates that no cracks, trenches, or pinholes are present in the coating. Positively charged hexaammine ruthenium ions can penetrate the film or even concentrate inside it, demonstrating pore accessibility after template extraction.[46,115−118] It is worth noting that both peak current and peak potential provide information about mass-charge transport processes. Peak current is associated with the concentration and diffusion of redox species in the film, while peak potential, as well as the shape of the voltammogram, can be used to differentiate between the diffusion of unbound redox species and electron hopping Finally, neutral probes (e.g., ferrocene methanol) can be used to test pore blockage or channel tortuosity (Figure 5).[119]

CV has also been used to get an estimation of the electroactive area not covered by the inorganic framework and the channel tortuosity in systems where the interactions between the redox probe and the channel walls are weak and the electrode surface is flat, so semi-infinite diffusion conditions can be assumed (i.e., the Randles−Ševčik equation can be applied). The approach has been used for nonsilica systems with large pores.[32] A brief discussion of those characterizations will be carried out in the following sections.[116]

3.1.2. MTFs as Sensors, Which Are the Relevant Parameters? The possibility of making films with the ability to exclude some species while preconcentrating others as well as controlling their transport inside the films has made MTFs a potentially attractive material for the development of electrochemical sensors. In this regard, a number of works have dealt with signal detection, exclusion, and electrode stability, which are crucial sensor parameters.

Silica MTFs tend to preconcentrate positively charged redox species under near neutral pH conditions. Preconcentration of Ag^+, hexaammine ruthenium, or ruthenium bipyridine has been reported by many authors.[46,98,114,116] However, there is an important difference in the preconcentration capacity when EASA- and EISA-derived MTFs are compared. Because of the pore orientation favorable to diffusion, EASA films with vertical channels are highly permeable to redox probes in the solution, and they are more likely to directly reach the electrode surface. The voltammograms obtained in EASA systems are comparable with those obtained in bare electrodes with free probes in solution and can be treated as diffusion in a semi-infinite electrode problem.[120,121] Regarding EISA-derived MTF, Brunsen et al.[110] and Alberti et al.[114] have observed that two forms of charge transport can coexist, i.e., by mass diffusion of unbound redox species and by electron hopping through the adsorbed species. This dual charge transport can be observed in the shoulder recorded at the multiple voltammograms presented in the cited works. However, so far, studies dealing with a sound comparison between both the EISA and EASA routes are lacking.

The observed mixed transport regime of probes inside the films and the already discussed aspects of lack of model precision are limitations to estimating the real parameters of interest, such as the diffusion coefficient or the redox species concentration in the pore systems and their relationship with the electrode performance. These parameters are relevant to the design and preparation of MTF-based sensor devices. The capacity of the preconcentration defines the limit of detection of a particular analyte in solution. Etienne et al.[116] reported that the preconcentration capacity must be different for 2D-hexagonal (*p6m*), 3D-hexagonal ($P6_3/mmc$), and 3D-cubic

https://doi.org/10.1021/acsomega.3c02013
ACS Omega 2023, 8, 24128−24152

(*Pm3n*) structures in silica MTFs and noted the difficulty to estimate the concentration of $Ru(bpy)_3^{2+}$ species accumulated in the film because its adsorption capacity is not known. In another work, Taffa et al. estimated the concentrations of $[Fe(CN)_6]^{4-}$ and $[IrCl_6]^{-2}$ inside the TiO_2 MTF, recording the current density as a function of the probe concentration, using a Langmuir-type isotherm.[122] Calvo et al. noted the high preconcentration capacity, mentioning that the high current values observed are related to a much higher concentration in the MTF than in the solution to satisfy the condition $j \propto D^{1/2}C$.[123] However, this assumption is true only in a diffusion regime where the Randles−Ševčik condition can be applied. DiMarco et al.[124] presented a method to determine the upper and lower limits, as well as one intermediate value of the distance between two ruthenium complexes inside the TiO_2 MTF to study the effect on the self-exchange intermolecular Ru(III/II) electron transfer, a process commonly referred to as "hole-hopping". For this estimation, assumptions about the porosity of the film and the close packed nature of the molecules were required. An electrochemical method to estimate the capacity of the MTF to preconcentrate $Ru(NH_3)_6^{3+}$ has been reported by determining the area for anodic or cathodic peaks in a support electrolyte solution after $Ru(NH_3)_6^{3+}$ loading, so the current can only correspond to the adsorbed species.[31] The authors reported a limit of detection of approximately 15 μM for $Ru(NH_3)_6^{3+}$. Similar limits of detection were reported for gases, redox probes, or volatile molecules sensing.[26,125−127]

Despite the extended use of the Randles−Ševčik equation to interpret transport and reactivity in MTFs, recent work has challenged this interpretation. Steinberg et al. studied and modeled the mass transport of electroactive species through the TiO_2 MTF by cyclic voltammetry.[112] The authors propose that the Randles−Ševčik interpretation within the framework of planar semi-infinite diffusion results insufficiently to properly describe the voltammetric curves. An alternative scenario can therefore be proposed, which considers that the access of redox species from the solution to the electrode can be affected by poor interconnectivity in the channels. As a result, some regions of the electrode could become inaccessible and, thus, electrochemically inactive. The authors proposed that such a partly blocked electrode could be modeled as an array of ultramicroelectrodes, following a model developed by Matsuda (see Figure 6).[128] Depending on the relationship between certain critical parameters (the area of the electroactive domains acting as ultramicroelectrodes; the average distance between them; neck and pores sizes; redox probe's size, charge, and diffusion length), the voltammetric response presented a transition which could be modeled in terms of that typical of planar semi-infinite diffusion (low blockage) to that of spherical semi-infinite diffusion (high blockage). Indeed, a similar behavior has been observed in the case of very thin zirconia membranes deposited onto Pt. These nanoperforated membranes behave as a nanoelectrode array and present different diffusion regimes that depend not only on the pore size but also on their interpore separation, demonstrating that the analytical signal can have a complex dependence of the electrode geometry and measuring conditions.[59]

4. BEYOND POSTSYNTHESIS MODIFICATION: TARGET ANALYTE SELECTION AND CONCENTRATION

4.1. Selective Principle. In principle, selectivity can be achieved by pore modification, which in turn changes mass transport within the nanopores. This can be done through the design of the film characteristics (mesostructure, pore size and orientation, and thickness) and/or the postsynthesis functionalization of the film.[28]

4.1.1. Molecular Sieves. Some relevant features of MTFs as perm-selective units are the extended pore size range, the absence of swelling, and the size selectivity. Kisler et al.[129] early reported the potential of MCM-41-containing molecular sieves to adsorb two proteins (lysozyme and trypsin) and a vitamin (riboflavin), obtaining an adsorption ratio strongly dependent on the relative size of the adsorbed molecule, with the smaller molecules (riboflavin) being those that were adsorbed faster. Mesopore size combined with functionalization has also been reported to filter out proteins present in plasma that could constitute interferences, improving analyte detection through SERS.[130]

Besides, an MTF on the electrode surface can be used as a molecular sieve to protect the electrode surface from biofouling, as shown in the work by Serrano et al.,[131] in which vertically aligned mesoporous silica generated at an ITO electrode surface by the EASA method prevented adsorption of undesired large size molecules (e.g., hemoglobin) while allowing the detection of small redox active molecules likely to reach the electrode surface through the film (e.g., propranolol) with almost no loss of sensitivity.

4.1.2. Medium Affinity. The MTF medium affinity is mainly determined by the density of silanol groups on the surface and can be adjusted by changing the mesopore wall polarity. Normally, MTFs are therefore poorly wet by organic compounds due to their surface polarity. However, compatibility with organic solvents can be achieved by adding organic building blocks to the inorganic matrix, either through subsequent modification of the pore surface of a purely inorganic silica material ("grafting"), through the simultaneous condensation of the precursors of corresponding silica and organosilicate ("co-condensation", also called "one-pot synthesis"), or by incorporating organic groups as bridging components directly and specifically in the pore walls through the use of bis-silylated single-source organosilica precursors.[28]

Ghazzal et al.[132] demonstrated how the hydrophobic−hydrophilic balance of the film can change the selectivity and sensitivity of an optical sensor for the adsorption of analytes with different chemical polarities (water and hexane). In this work, mesoporous dielectric multilayers of SiO_2/TiO_2 were developed, but the hydrophilic−hydrophobic balance occurs in the mesoporous SiO_2 layer, which was synthesized by a co-condensation of mixtures of methyltriethoxysilane (MTES) and tetraethyl orthosilicate (TEOS). A gradual increase in the hydrophobic behavior of the hybrid silica layer was observed, obtained by increasing the methyl group content. The authors found that water molecules remained outside the silica layers due to the surface affinity, while hexane penetrated more easily due to its affinity to the hydrophobic silica pore surface.

Yan et al.[133] proposed a highly selective and sensitive method to electrochemically detect traces of nitroaromatic compounds, such as explosives and organophosphate pesticides (OPs) but using another approach to modify the MTF

https://doi.org/10.1021/acsomega.3c02013
ACS Omega 2023, 8, 24128−24152

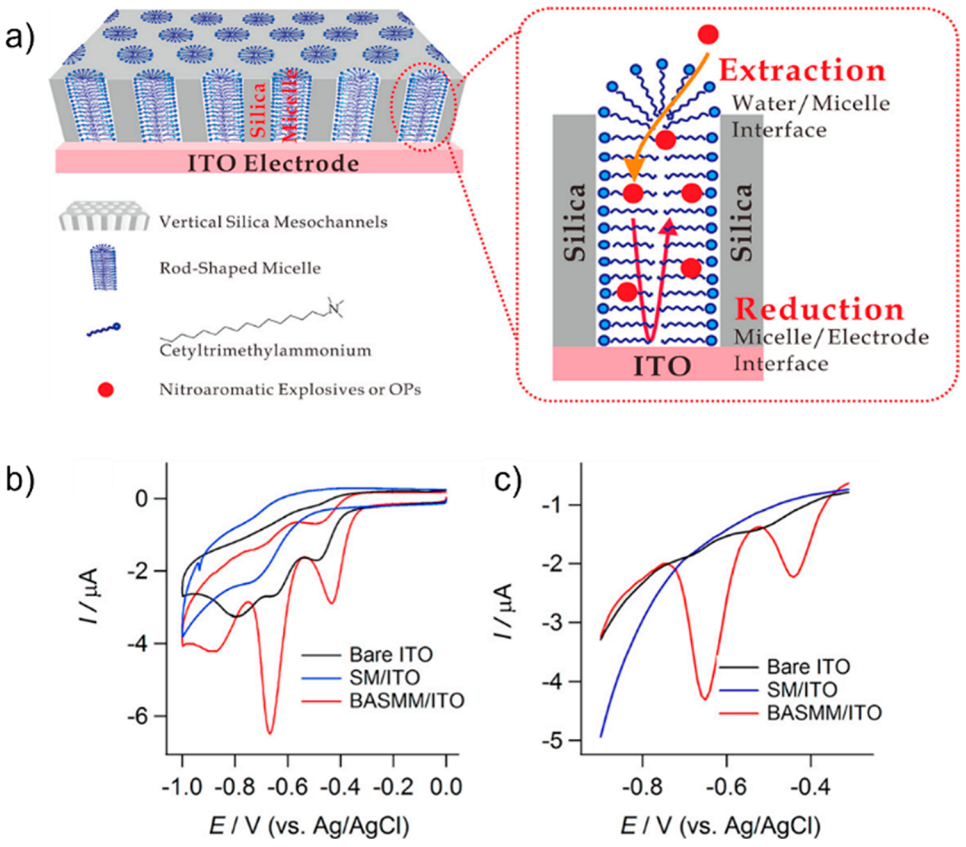

Figure 7. (a) Representation of nitroaromatic explosives and OPs electrochemical analysis at a binary assembly of silica mesochannels and micelles in a BASMM/ITO electrode. (b) CVs of 1 ppm TNT and (c) DPVs of 200 ppb TNT at the bare ITO (black), silica mesochannels/ITO (blue), and BASMM/ITO (red) electrodes in 0.5 M NaCl. The scan rate was 10 mV s^{-1}. Reprinted with permission from F. Yan et al. *Anal. Chem.* **2015**, *87*, 4436−4441. Copyright 2015, American Chemical Society, ref 133.

affinity with the medium. This method consisted of the use of ITO electrodes modified with a highly ordered and aligned binary assembly of silica mesochannels and surfactant micelles (Figure 7). The modified ITO electrode surface can provide rigid and robust support to confine the soft cylindrical micelles formed by the aggregation of the cationic template cetyltrimethylammonium bromide (CTAB), whose tails make each micelle have a hydrophobic core, which acts as an excellent adsorbent for rapid extraction and preconcentration of trace nitroaromatic compounds from aqueous solutions via the hydrophobic effect.

4.1.3. Charge-Based Selection. As mentioned above, the ionic strength affects the Debye length in the mesochannel. This was studied in detail by Nasir et al.,[30] who deposited vertically aligned mesoporous silica thin films onto glassy carbon electrodes (GCEs) by EASA with the aim of electrochemically detecting the herbicide Paraquat in aqueous samples. When the potential distribution across the mesochannel is negative, Paraquat accumulates within the mesochannel. As the solution pH increases, the silica surface becomes more negatively charged, and the absolute zeta potential increases; therefore, an increase of the Paraquat concentration within the mesochannels occurs. However, when I < 70 mM, a drop in the reduction peak current is observed. This can be linked to the overlap of the double layers, leading to the exclusion of anions from the mesochannels, as discussed above.

Taffa et al.[134] showed how this effect increases if the mesochannels are functionalized, because functionalization affects the "free" pore diameter. For example, strong current suppression was observed in functionalized mesochannels with long alkyl chains and redox ions possessing large negative charges. These observations agree with a Debye layer extending from the charged pore wall toward the center of the pore and building up an electrostatic barrier, which increases with the membrane thickness and depends on the concentration of the inert electrolyte. Moreover, Fattakhova-Rohlfing et al.[33] synthesized organized mesoporous layers of SiO_2 with a template-assisted procedure using a Pluronic F127 block copolymer template. This MTF was uniformly functionalized with protonated amino groups and exhibited excellent permselective membrane properties, which can be reversibly controlled by pH changes.

More complex systems can be synthesized to create properties that emerge from the synergy among the components. Calvo et al. synthesized mesoporous silica thin films on silicon and ITO substrates, which were then modified by growing zwitterionic poly(methacryloyl-L-lysine) (PML) brushes.[111] In this system, a property arises that differs from the sum of the component properties (Figure 8). The IEP of the zwitterionic brush is ∼5, and as such, it is expected that at pH > 5 the nanopore is negatively charged (cation-permselective), and at pH < 5 it is expected to be positively charged (anion-permselective). However, at pH < 5, the PML brush-modified mesoporous film acts as an ionic barrier, and that is because, in the pore walls, the grafted polyzwitterionic chains coexist with silanol sites, which are negatively charged at pH > 2, so the nanopore is "bipolarly charged". The interesting

https://doi.org/10.1021/acsomega.3c02013
ACS Omega 2023, 8, 24128−24152

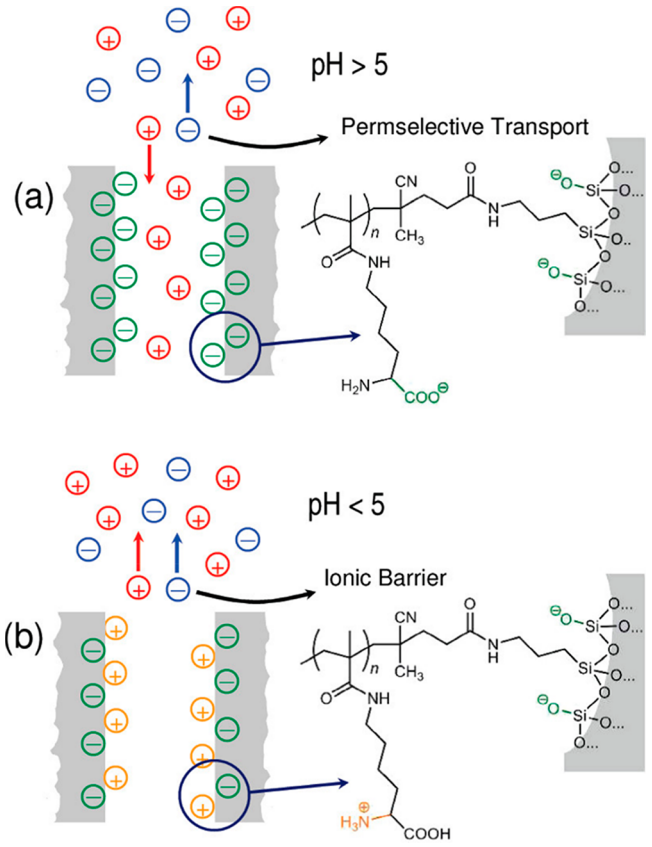

Figure 8. Schematic depiction of the ionic transport processes taking place in the hybrid assembly of mesoporous silica thin films modified with zwitterionic poly(methacryloyl-L-lysine) brushes at (a) pH > 5 and (b) pH < 5. Reprinted with permission from A. Calvo et al. *J. Am. Chem. Soc.* **2009**, *131*, 10866−10868. Copyright 2009, American Chemical Society, ref 111.

result is that the confinement of both negative and positive charges leads to a very particular exclusion condition, in which initially the anions are attracted to the pore by the positive charges in the "bipolar" wall, but the negative charges of the "bipolar" wall are close to the positive ones, and as a result, repulsion of the anions occurs simultaneously.

A relevant factor affecting the surface charge is the ionic strength. Taffa et al.[134] studied the pore size and surface charge control in mesoporous TiO_2 using a postgrafted organic self-assembled monolayer. The addition of the non-electroactive salt $LaCl_3$ to the electrolyte solution leads to La^{3+} adsorption due to the presence of sulfonate head groups in the membrane. Adsorption of La^{3+} generates a surface charge inversion visualized by conducting electrochemical detection experiments with $[Fe(CN)_6]^{4-}$ and $[IrCl_6]^{2-}$. The currents increased with increasing La^{3+} concentration until they reached a similar value as on unmodified TiO_2, but a further increase in the concentration of La^{3+} ion resulted in a slight decrease of the current.

Both factors can be exploited for electrochemical detection applications. Jiokeng et al.[135] developed amino-attapulgite (Amino-AT)/mesoporous silica composite films generated by electroassisted self-assembly for the voltammetric determination of diclofenac (DCF), in which the Amino-AT can enhance the DCF oxidation signal and improve electron transfer rates, suggesting the existence of both accumulation and electrocatalytic effects. The obtained responses were strongly pH-dependent, and this was attributed to the acid−base properties of DCF, the surface charge of AT and Amino-AT, and the oxidation mechanism of DCF. The Square Wave Voltammetry response of DCF at an Amino-AT-modified glassy carbon electrode was also influenced by the ionic strength. Peak currents were first found to increase, reaching a maximum at 0.10 M NaCl, and then decreased continuously for larger ionic strength values, which indicates that there is an impediment to the accumulation of the negatively charged DCF due to competition with the electrolyte anion (Cl^-) for the binding sites of protonated Amino-AT. Also, lower intensities observed in more diluted solutions could be due to increased solution resistance.

Yan et al.[136] recently developed phenylboronic acid-functionalized vertically ordered mesoporous silica films (PBA-VMSF), grown on ITO electrode using the Stöber solution growth approach, for selective electrochemical determination of fluoride ion in tap water. They took advantage of the MTF preconcentration ability to make indirect detection. As the boronic acid moiety can selectively bind to F^-, the negative charges rise, electrostatically excluding the ferricyanide anions through the ultrasmall silica nanochannel to the underlying electrode. Therefore, the decreased redox response of $Fe(CN)_6^{3-}$ is related to the amount of F^-.

Similarly, Karman et al.[137] developed an indirect detection method, focused on amplifying the voltammetric responses of anionic redox probes ($Fe(CN)_6^{3-/4-}$), which are usually prevented/limited at mesoporous silica film-modified electrodes. This method consisted of using neutral or positively charged solution-phase redox mediators ($Fc(MeOH)_2$ or $(Ru(NH_3)_6^{3+}$) that are likely to diffuse freely through the membrane to the electrode surface. These two probes experience reversible and one-electron redox reactions; also, both couples ($Fc(MeOH)_2/Fc(MeOH)_2^+$ and $Fe(CN)_6^{4-}/Fe(CN)_6^{3-}$) are characterized by very similar standard potential values. The amplification of $Fe(CN)_6^{4-}$ oxidation was clearly due to the $Fc(MeOH)_2$ acting as a redox mediator:

$$Fc(MeOH)_2^+ + Fe(CN)_6^{4-} \rightleftharpoons Fc(MeOH)_2 + Fe(CN)_6^{3-}$$

The $Fc(MeOH)_2$ molecules were easily diffusing through the mesoporous silica film, so they were oxidized onto the underlying ITO surface, into $Fc(MeOH)_2^+$ species, which can diffuse back through the film, thus becoming available for oxidizing the charge-excluded solution-phase $Fe(CN)_6^{4-}$ species.

4.2. Combined Selective Principles. The selective principles mentioned above are not isolated phenomena; therefore, an electrochemical detection system using MTFs may have a combination of them.

4.2.1. Pore Size and Probe Charge. Vilà et al.[138] studied the combined effect of pore size and charge by analyzing the permeability of Dawson-type polyoxometalates through vertically oriented nanoporous silica membranes templated by CTAB and larger-size octadecyltrimethylammonium bromide (ODAB) deposited onto an ITO electrode. These experiments were carried out at various ionic strengths and in an acidic medium, where the silica surface is positively charged and thus likely to interact with the negatively charged redox probes. The permeability of negative probes through the positively charged silica pores was also affected by the electrolyte concentration. The "effective pore size" is

https://doi.org/10.1021/acsomega.3c02013
ACS Omega 2023, 8, 24128−24152

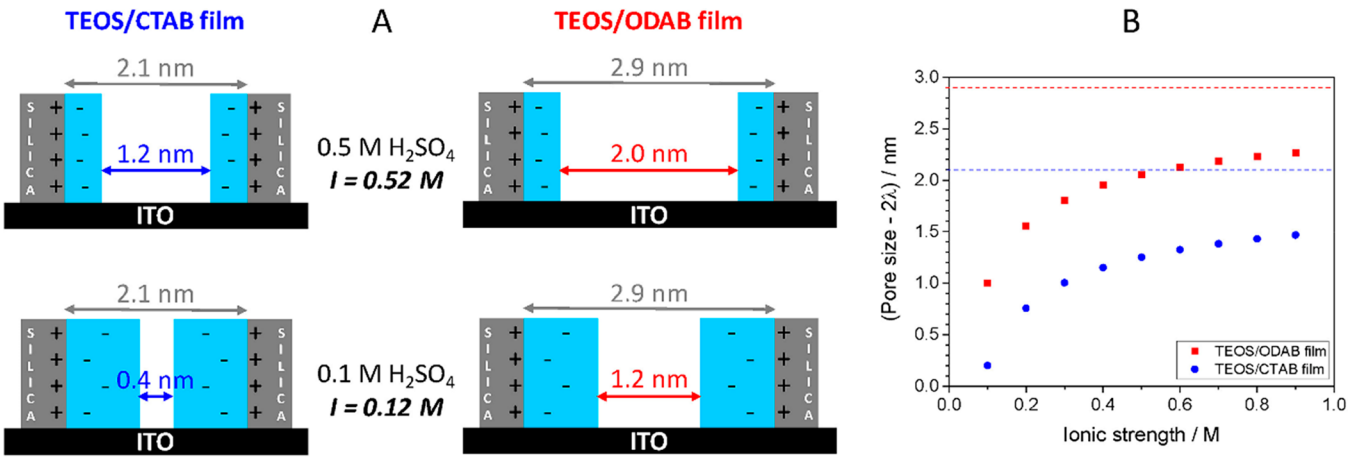

Figure 9. (A) Schematic view of mesopore channels of CTAB- and ODAB-based films with electrical double layers corresponding to pH 0.3 and 1.0. (B) Variation of the effective pore diameters as a function of the ionic strength (dashed lines represent the pore diameter of both mesoporous films). Reprinted with permission from N. Vilà, et al. *Electrochim. Acta* **2020**, *353*, 136577. Copyright 2020, Elsevier, ref 138.

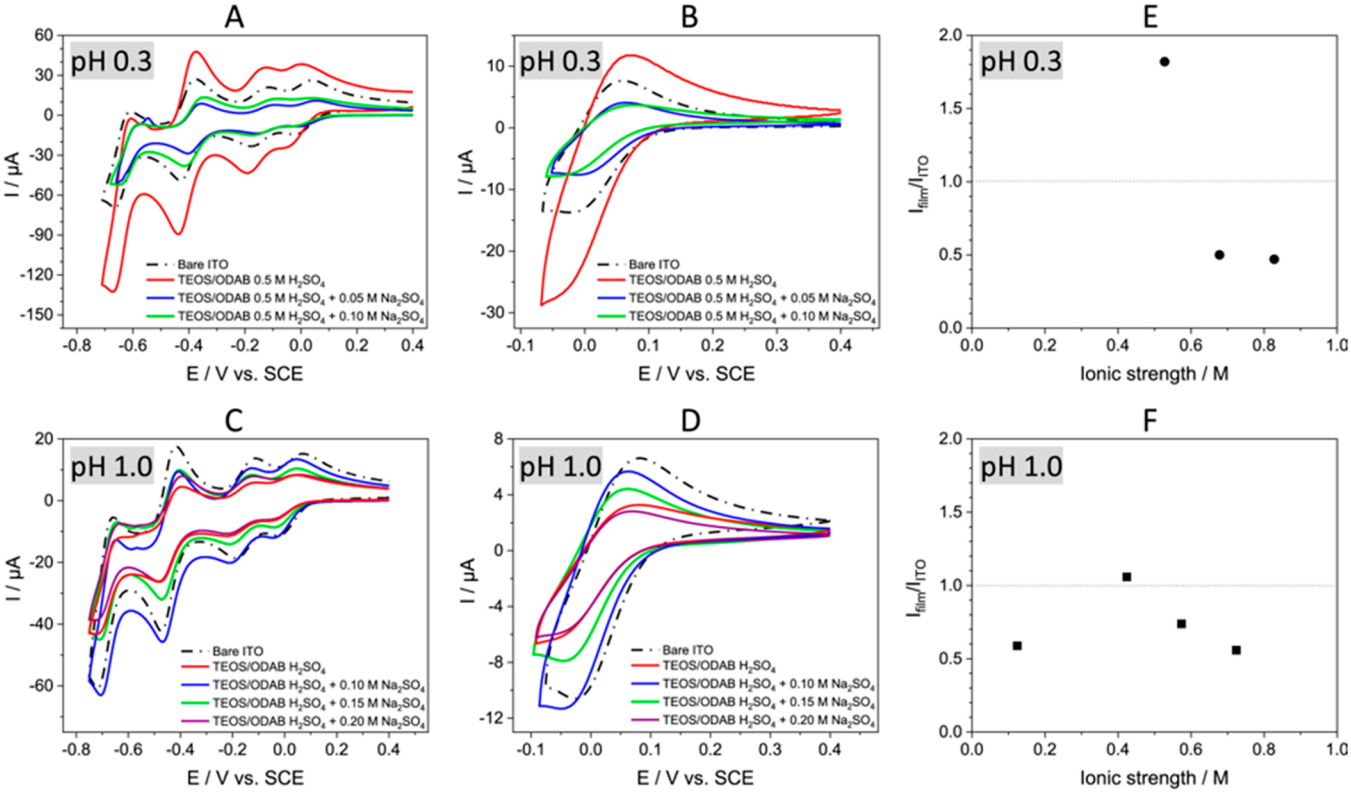

Figure 10. (A–D) Voltammograms recorded in a solution containing 0.5 mM of $[P_2W_{18}O_{62}]^{6-}$ and H_2SO_4 at concentrations adjusted to fix the pH to 0.3 or 1.0 and Na_2SO_4 added at selected concentrations (0.10, 0.15, or 0.20 M), using a bare ITO electrode and ITO covered with an ODAB-based mesoporous silica film at 20 mV s^{-1}. (E and F) Peak current ratio variation between film and bare electrodes (I_{film}/I_{ITO} values) as a function of the ionic strength. Working electrode area: 0.125 cm^2. Reprinted with permission from N. Vilà et al. *Electrochim. Acta* **2020**, *353*, 136577. Copyright 2020, Elsevier, ref 138.

determined by the pore diameter and the thickness of the electrical double layer (Figure 9). The $[P_2W_{18}O_{62}]^{6-}$ species were likely to cross easily the ODAB-based film and even to accumulate inside, but their response at the CTAB-based film electrode was much less intense and even lower than at bare ITO, which can be explained by the smaller pore diameter of the CTAB-based film. This effect was even more noticeable and restrictive at pH 1.0, indicating a pH-influenced size selectivity of the mesoporous films. It is worth noting the similarity in the intensity of the voltammetric signals of $[P_2W_{18}O_{62}]^{6-}$ at the small pore film at pH 0.3 and the the larger pore film at pH 1, both situations corresponding to the same "effective pore diameter" (Figure 10).

4.2.2. Medium Affinity and Probe Charge. Taffa et al.[139] worked with sintered mesoporous TiO_2 thin films, on which inner walls were grafted with alkyl phosphonic acids (Pho-Cn-R) of different chain length (6, 10, and 14 carbons) with neutral, positive, and negatively charged head groups (R = -H, R− = sulfonate, R+ = pyridinium). The neutral phosphonic acid modifier makes the TiO_2 highly hydrophobic and

https://doi.org/10.1021/acsomega.3c02013
ACS Omega 2023, 8, 24128−24152

suppresses electrochemistry in aqueous media, and the alkyl phosphonic acids with charged head groups render the TiO_2 film as an ion exchanger with a phase separated hydrophilic and hydrophobic portion. Different charged guest molecules were incorporated on top of or into the supported membranes. The host−guest interactions were found to be electrostatic, hydrophobic, or both. Depending on their carbon chain length, they occupied a considerable space of the average pore volume (ca. 5−10%). Their head groups (R) determine the "inner-wall" surface properties and potential interactions with species in solution.

4.2.3. Medium Affinity, Pore Size, and Probe Charge. Yan et al.[140] combined these selection principles to achieve a direct electrochemical detection of electroactive small organic analytes in complex media without sample pretreatment. ITO electrodes were modified with permselective membranes consisting of vertically ordered silica mesochannels and surfactant micelles (OSM@SM). These membranes were only permeable to small and neutral/hydrophobic molecules, because of the size of SMs and lipophilic cores of OSMs. CV and differential pulse voltammetry in soil dispersions containing paraoxon show no or only an ill-defined current response at the bare ITO and SM/ITO electrodes. In contrast, the electrode displays a well-defined reduction current peak due to reduction of the nitro group. The results indicate that the OSM@SM layer can effectively block the access of large substances, such as soil particles and other contaminants, to the underlying ITO surface, in addition to extracting and concentrating paraoxon from the soil dispersion.

Table 3 shows a comparison of some analytical figures of merit for some reported mesoporous film-based sensors. As can be seen, MTF-modified sensors have been used both for simple ions and for more complex molecules. From the information reported in these studies, the sensitivities and detection limits are consistent for each analyte. However, few studies report information on the reproducibility of the measurements. This is a key issue for real sensor applications beyond proof-of-concept. Sensor-to-sensor reproducibility, for example, is crucial when considering scaling up; batch-to-batch reproducibility is also relevant in order to assess the soundness of the preparation protocols. In addition, repeatability of the sensor response after prolonged use or washing is also an essential performance indicator (i.e., whether a device can be washed and reused or if the sensor is irreversibly damaged after a single measurement). In this context, the long-term stability becomes a very important parameter. Most studies have been conducted on silica films, which present relatively high solubility even in mildly acidic or neutral pH. Recent studies show that transition metal oxide films are much more stable in solution, and doping with even small quantities (2−10%) of Zr(IV) or Ti(IV) notably enhances the electrode stability in solution.[114,148]

In summary, three typical approaches are employed to take advantage of the basic MTF properties such as large specific surface area, adsorption, electrostatic preconcentration or exclusion, steric or phylic modification, and size sieving.

First, when preconcentration in the channels (by electrostatic adsorption, complexation, lipophilicity, etc.) is the main goal, the analyte must be an electroactive species that undergoes an electron transfer reaction at the surface of the electrode. This process is usually followed by voltammetry (mainly SWV), and the peak current follows a linear relationship with the analyte concentration. This approach has been used intensively. For a MTF-coated electrode, a linear range falling in a region between approximately 1 μM and 1 mM is usually obtained.[131,135,143,149] However, when MTFs are used in combination with other electrocatalytic materials presenting high surface area, such as graphene, lower LOD and wider dynamic ranges can be obtained (for instance, LOD values close to 1 nM have been reported[150]).

A second approach involves filling the channels with a redox mediator. In this case, a redox reaction takes place between the analyte and the redox mediator.[142,151] The charge transport is then completed by electron hopping between the redox mediators in the channel and electron transfer at the electrode. As in the previous case, the analytical signal usually is acquired by voltammetry, and again, a linear relationship between current and concentration is obtained. However, in this case, if the electron transfer reaction between the analyte and the redox mediator takes place only at the mesoporous film/solution interface, the high surface area provided by the MTF channels is not fully exploited, and LODs are usually between 1 and 10 μM, with a linear range in a region between approximately 1 μM and 1 mM.

Finally, a less explored approach consists of the adsorption of a non-electroactive analyte, e.g., fluoride, which blocks the entrance of an electroactive species (e.g., ferricyanide) into the channels and prevents its electrochemical reduction or oxidation. In order to compete for electrostatic adsorption, both species must have the same charge sign and be electrostatically attracted to the channel walls. When this process is followed by voltammetry, there is a decrease in the voltammetric peaks as the concentration of the analyte is increased. The peak current usually follows a logarithmic dependence with the concentration, and therefore, the determination of the concentration may be affected by a relatively high error. However, low LODs and wide dynamic ranges (several orders of magnitude) can be achieved.[136]

5. FURTHER APPLICATIONS IN BIOSENSING

Biosensors are compact analytical devices conformed of three components: a biorecognition element, a transducer, and an associated electronic circuit to process and display the result of the measurement. The interaction of the analyte with a specific biorecognition element attached to the surface of the transducer results in changes in properties (e.g., optical, electrochemical, or gravimetric) which can be converted by the transducer to an electrical signal related to the analyte concentration. Electrochemical transducers are the preferred option in biosensing because they directly convert the recognition event into an electrical signal, which allows for integration, miniaturization, and reduced fabrication costs.[152,153]

The choice of the biorecognition elements is dictated by the nature of the analyte. For instance, small organic molecules with redox properties, such as glucose and lactate, are usually detected with an appropriate redox enzyme (e.g., glucose oxidase and lactate oxidase, respectively), and the result of the catalytic activity is transduced to a current proportional to the reaction rate. On the other hand, larger biomolecules are usually detected by affinity biosensors, where the biorecognition element is usually an antibody or an aptamer immobilized on the surface of the transducer, and the formation of complexes with the target analyte is detected by different techniques (voltammetry, electrochemical impedance, etc.) according to the biosensor design. In both cases, there have

https://doi.org/10.1021/acsomega.3c02013
ACS Omega 2023, 8, 24128−24152

Table 3. Comparison of Some Currently Reported Mesoporous Film-Based Sensors

	Electrode modification	Analyte	Detection technique	Sensitivity	Linear range	LOD	Reproducibility	Long-term stability	Ref
Electrocatalysis	Carbon paste electrode modified with mesoporous silica encapsulating polyaniline decorated with gold nanoparticles	Ascorbic acid	Differential pulse voltammetry	95.95 μA mM^{-1}	0.005−13.3 mM	0.97 μM	-	2 weeks (93−94% of its initial response)	141
	Mesoporous silica thin film encapsulating iron-triazole complex by EASA on ITO electrode	Hydrogen peroxide	Amperometry	1.9 A mol^{-1} cm^{-2}	5−300 μM	2 μM	-	-	142
Preconcentration	Aminopropyl-functionalized MCM-41 and SBA-15 powders coated with Nafion to modify GCE	Cadmium ion	Square wave anodic stripping voltammetry	MCM-41: 765 ± 20 μA mM^{-1} SBA-15: 1520 ± 20 μA mM^{-1}	MCM-41: 0−10 μM SBA-15: 0−10 μM	MCM-41: 0.71 μM SBA-15: 0.36 μM	4 measurements with a RSD of 5.87%	-	143
Charge selective effect	Mesoporous silica thin film by EASA on ITO electrode and postgrafted with ammonium groups	Ascorbic acid (AA) and dopamine (DA)	Differential pulse voltammetry	-	AA: 49−2651 μM DA: 20−226 μM	AA: 11 μM DA: 9 μM	-	-	144
	Mesoporous silica thin film by Stöber-solution growth approach on ITO electrode	Methylene blue	Differential pulse voltammetry	-	10 nmol L^{-1}−1.0 μmol L^{-1}	4.10 nmol L^{-1}	-	-	145
	Mesoporous silica thin film by EASA on GCE	Paraquat	Square wave voltammetry	21000 μA mM^{-1}	10−40 nM	12 nM	-	-	30
	Amino-attapulgite/mesoporous silica film by EASA on GCE	Diclofenac	Square wave voltammetry	125 μA mM^{-1}	0.3−20 μM	0.053 μM	6 parallel detections with a RSD of 5.62%	-	135
	Phenylboronic acid-functionalized mesoporous silica film by Stöber-solution growth approach on ITO electrode	Fluoride ion	Differential pulse voltammetry	-	1 × 10^{-9}−1 × 10^{-3} M and 1 × 10^{-3}−2.3 × 10^{-2} M	8.3 × 10^{-10} M	-	2 months	136
	Ferrocene-functionalized mesoporous silica film by EASA on ITO electrode	Cysteine	Chronoamperometry in flow cell	1.28 μA mM^{-1}	3- 20 μM	3 μM	RSD of 3−12%	-	146
Size selective effect	Mesoporous silica film by EASA on ITO electrode	Propranolol	Cyclic voltammetry	67.4 ± 7.2 mA mol^{-1}	5−100 μM	5 μM	-	-	131
	Mesoporous silica film by EASA with electrochemical reduced graphene on GCE	Doxorubicin	Differential pulse voltammetry	7815 μA mM^{-1}	0.001−20 μM	0.77 nM	Continuous detections within 24 min and no apparent current variations were observed	-	147
Lipophilicity selective effect	Mesoporous silica film by Stöber-solution growth approach on ITO electrode without surfactant elimination	Nitroaromatic compounds (explosives and organo-phosphate pesticides)	Differential pulse voltammetry	TNT: 2318.99 ± 29.53 μA mM^{-1} DNT: 1573.60 ± 21.85 μA mM^{-1} TNP: 7958.93 ± 442.16 μA mM^{-1} NP: 546.70 ± 12.52 μA mM^{-1} NB: 437.04 ± 6.15 μA mM^{-1} Paraoxon: 3951.87 ± 167.87 and 1406.27 ± 79.81 μA mM^{-1}	TNT: 10−1000 ppb DNT: 10−1000 ppb TNP: 2−80 ppb NP: 40−2000 ppb NB: 10−3000 ppb Paraoxon: 5−385 and 385−2000 ppb	TNT: 4.97 ± 0.06 ppb DNT: 5.87 ± 008 ppb TNP: 1.46 ± 0.08 ppb NP: 12.90 ± 0.30 ppb NB: 14.28 ± 0.20 ppb Paraoxon: 3.53 ± 0.15 ppb	-	-	133

https://doi.org/10.1021/acsomega.3c02013
ACS Omega 2023, 8, 24128−24152

Table 3. continued

Electrode modification	Analyte	Detection technique	Sensitivity	Linear range	LOD	Reproducibility	Long-term stability	Ref
			Methyl parathion: 4902.58 ± 119.43 and 2939.22 ± 61.17 $\mu A\ mM^{-1}$	Methyl parathion: 5−136 and 136−1000 ppb	Methyl parathion: 3.01 ± 0.07 ppb			
			Fenitrothion: 121.98 ± 2.77 $\mu A\ mM^{-1}$	Fenitrothion: 400−7000 ppb	Fenitrothion: 114.86 ± 2.68 ppb			

been a considerable number of studies where mesoporous thin films have been incorporated to improve the performance of electrochemical biosensors.

Electrochemical biosensors can benefit from the inclusion of mesoporous films, improving sensitivity, LODs, selectivity, and stability. For instance, the mesoporous structure of the film provides a high surface area, which can be used to immobilize a large amount of biorecognition elements, resulting in higher sensitivity and improved detection limits. Additionally, the porous structure of the films composed of biocompatible materials, such as silica, can also improve the stability and activity of the biorecognition elements by reducing their exposure to harsh environmental conditions. Finally, the mesoporous structure can also reduce nonspecific binding and exclude interferents or other molecules present in the sample, which can improve the specificity of the biosensor. Due to these enhancing possibilities, mesoporous thin films have been incorporated into the design of different electrochemical biosensors.

The characteristics of MTFs and their associated electrochemical processes have found applications in the development of different kinds of electrochemical biosensors. Silica MTFs (SMTFs) are especially attractive materials for the development of electrochemical biosensors because of their biocompatibility, high specific area, controllable pore structure and size, and easy surface modification with chemical groups or biomolecules. Titania and zirconia MTFs also present excellent biocompatibility and have been used in the construction of biosensors, although to a lesser extent since their chemistry is less extended. However, pore control and surface functionalization are also simple and reproducible through different chemical pathways.[58,154]

Different strategies have been used to take advantage of the versatility of MTFs according to the analyte and the type of biological recognition elements. Regarding electrochemical biosensors, two approaches have been used that involve the immobilization (by adsorption, covalent bonding, entrapment, or other means) of the biorecognition elements either on the outer surface of the MTF or in its pore systems (Figure 11). Mesoporous structure, pore size and structure, surface functionalization and charge, and hydrophilicity are relevant MTF features that can be tuned to improve enzymatic stability and activity.[26,155] A critical aspect in order to immobilize enzymes inside the SMTFs is the mesopore size. Typically, lower enzyme loadings are obtained for larger pores, since the specific surface area decreases with increasing pore size. It has been noted that a pore size similar to or slightly greater than that of the enzyme can not only lead to higher loading capacity but also preserve the catalytic activity of the enzymes since unfolding and denaturation are restricted by the MTF framework. In brief, the pore and interfacial characteristics must be adjusted to achieve high enzyme stability and loadings.

In addition to the incorporation of enzymes, the mesoporous structure can be used to incorporate electroactive species or conductive components.[156] The co-immobilization of enzymes with electrocatalytic metallic NPs or the incorporation of redox mediators has been assayed in order to overcome the insulating characteristics of silica and enhance electron transport toward the electrode. Several synthetic aspects have to be optimized in order to successfully combine enzyme activity and charge percolation through the conductive species, which is applicable to sensors as well as other electroactive MTF-based electrodes.[157−159]

https://doi.org/10.1021/acsomega.3c02013
ACS Omega 2023, 8, 24128−24152

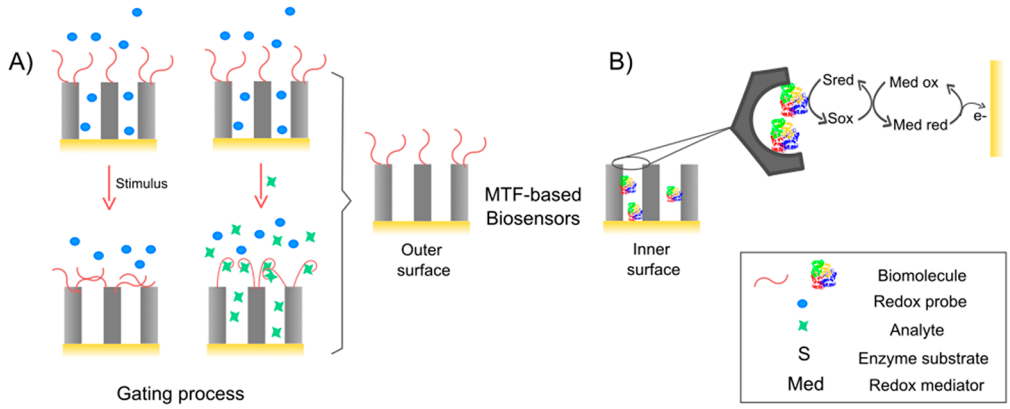

Figure 11. (A) Scheme of an MTF-modified electrode modified with a gating surface component (e.g., a responsive polymer or aptamer) on the surface. (B) Scheme of an enzyme-modified mesopore and the principle of analyte detection.

Regarding immunosensors, capture assays using an enzymatic label conjugated to a secondary antibody in combination with a redox mediator are a widely used strategy in electrochemical biosensors, in which high sensitivity can be achieved thanks to the high loads of immobilized antibodies on the surface of mesoporous materials.[160]

One of the most potentially interesting approaches for biosensors using MTF electrodes is based on gating processes that involve capping the nanochannels with an active component that might assist biorecognition in response to an external signal (Figure 11).[161] Strategies have been developed for biosensors based on biorecognition events blocking or unblocking the flux of redox probes through the nanochannels to the underlying electrode. In this kind of label-free, on−off sensors, the recognition event acts as a gate for the electrochemical signal generation of the redox reporters.[162] Different events may act as gating processes, and this approach has been employed in enzymatic and affinity biosensors, using biorecognition elements.

For instance, aptamers are valuable biorecognition elements. The formation of aptamer−target complexes on MTF surfaces promotes blockage of the MTF channels, inhibiting the transport of redox species, which can be detected by voltammetry or electrochemical impedance as a decrease in current peaks or an increase in the charge transfer resistance. This approach has been used for the detection of Prostate-Specific Antigen using electrochemical aptasensors, in which aptamers blocked the channel after target recognition.[127] While many of the gated biosensors are based on blocking the passage of redox species in solution after the recognition event, Lee et al. reported a different approach based on the release of methylene blue loaded in MTFs following the formation of detachable aptamer−avian influenza virus complexes. The sensing platform included a second MTF electrode capped with a control aptamer, which did not react with the target, to provide a baseline and correction to drifts due to interferences.[163]

Finally, field-effect transistor (FET) biosensors based on nanomaterials such as silicon nanowires[164] and graphene[165] have the potential of rapid and label-free detection of a wide range of biomarkers. Indeed, FET biosensors detect changes in the charge distribution at the surface of the transistor when biomolecules bind to the biorecognition elements on the gate electrode or the transistor channel.[152] This change in the electrostatic potential is then used to transduce the signal. However, mobile ions in the solution can screen for this electrostatic potential. For instance, the Debye screening length under physiological conditions is below 1 nm, while biorecognition elements and target analytes typically have sizes of several nanometers. MTFs have been proposed as a means to expand the field-effect length. Recently, silica MTF coatings on graphene-based FETs were found to provide amplified and extended field-effect sensing.[166] The extension and amplification of the field effect have been explained in terms of the increase of the Debye screening length in the mesoporous film, which in turn is caused by the decrease of free ions inside the pores due to Donnan exclusion. Additionally, the MFTs could benefit from another mesoporous property such as size exclusion, which resulted in improved selectivity toward the detection of molecules smaller than the pore size.

This section is far from being exhaustive on the applications of MTFs in the biosensor field, which is advancing at a very fast pace. New strategies for the design of biosensors are constantly reported taking advantage of the characteristics and versatility of biofunctionalized MTFs, especially in combination with other nanomaterials and hierarchical structures.[29,167]

6. INTEGRATION OF INTEGRATED CIRCUITS AND MICRO-ELECTROMECHANICAL SYSTEMS FOR ELECTROANALYTICAL APPLICATIONS

In the previous sections, we focused on the most relevant aspects of the synthesis, development, and characterization of MTFs for analytical applications. Here we move out from the chemistry and physics of MTFs to study the integration of these systems in the semiconductor industry to produce sensors on a large scale. There are three basic elements that must be integrated to obtain a completed functional device, which can be of amperometric or potentiometric type: the electrodes, the mesoporous thin film, and the associated electronic circuitry (e.g., potentiostat or potentiometer). For the assembly of this kind of device, two configurations can be chosen: either a modular integration of the components or a full integration into a single integrated circuit (IC). The modular approach is the most commonly used one. It is based on manufacturing the electrodes and then making the deposits of MTFs by some of the aforementioned methods. The working electrode (WE) and the counter-electrode (CE) can be made of ITO, FTO, Au, or C (the performance depends on the analytical requirements), and an external reference electrode (RE) is used, generally an Ag/AgCl reference

https://doi.org/10.1021/acsomega.3c02013
ACS Omega 2023, 8, 24128−24152

electrode. This configuration is very flexible since, in general, the potentiostat can be configured for using different electrochemical techniques and experimental parameters (cyclic voltammetry, square wave voltammetry, differential pulse voltammetry, impedance spectroscopy, etc.). There are very interesting works in which mesoporous films could be easily integrated into point-of-care (POC) devices. Potentiostats can be found in the literature with ad-hoc electronics that use a complete three-electrode cell (WE + CE + RE) made of disposable strips coated by screen printing or based on commercial electrodes.[168,169] This approach is based on manufacturing portable, inexpensive devices with specific ranges of electrode potentials and currents in which a mesoporous film could be easily deposited on the electrodes. A higher level of integration is achieved with the integration of the potentiostat, the electrodes, and the mesoporous film in the same silicon die. There are some very interesting works about the integration of working electrode arrays with a potentiostat in the same device, for health applications,[170] with modified surfaces,[171] or for multiple uses.[172−175] In this case, foundry facilities could be used to integrate a mesoporous film in these electrodes, considering that the precursors and condensation temperature can be adapted to its standard integrated microfabrication processes. However, the most serious problem lies in the integration of the reference electrode, since there are no studies in the literature that achieve a satisfactory integration of a RE in an IC. The integration of a RE is not easy due to the complexity of the electrode itself. In this sense, the use of inkjet techniques for printing a RE, such as that presented by Moya et al.,[176] may provide an approach to a complete integration of electrochemical sensors based on MTFs.

7. CONCLUSIONS AND OUTLOOK

After 20 years of their first reported synthesis, several pathways have been developed to produce and integrate mesoporous thin films as components of selective electrodes. In particular, EISA and EASA processes lead to straightforward fabrication and swift integration on metal or semiconductor electrodes. MTF chemical composition and pore size can be optimized for robust and highly accessible and addressable electrodes. This has spurred a new field, and the central questions are being answered convergently from several disciplines: materials, physical and analytical chemistry, bioscience, and materials science. Important advances have been made in the control of composition, pore diameter, structure, and functional surface control. Concerning synthetic aspects, the next directions will probably imply combining patterned microelectrode arrays with MTFs presenting localized control of functionalization (i.e., with arbitrarily located molecular, biomolecular, or nano species in the micron−submicron scale), in order to generate arrays of specifically responsive MTF-functionalized electrodes that give rise to analytical signatures. In addition, the development of low-temperature methods to deposit MTFs on flexible substrates is desired, in order to exploit these technologies in wearables or textile-embedded sensors. The use of artificial intelligence (AI)tools in the design, synthesis, and signal interpretation of these analytical systems will be desirable, in order to generate artificial tongues able to deal with complex matrices.

The unique feature of MTFs (and the more explored so far) is their role as a highly tunable perm-selective thin layer that excludes undesired molecules (interferences, electrode fouling agents, large molecules) and that preconcentrates the desired analyte. Harnessing pore size and interconnectivity, as well as tailoring pore surface and interior, gives a wide palette of possibilities to exploit selective pore and electrode accessibility through size sieving, and the use of electrostatic or intermolecular interactions. Thus, a new sensitivity and selectivity toolbox that exploits steric exclusion and preconcentration effects emerges from mesopore confinement and surface functionalization. The initial efforts have led to robust electrodes with high-quality signals and reasonable limits of detection and quantification, even if the signal generation and analyte/interference processes involved are still not completely understood.

It is important to stress that both the EISA and EASA processes lead to accessible mesopore systems. Since the beginning of the field, the slow preconcentration and complete exclusion behaviors observed on a mesoporous silica electrode were ascribed to the horizontal orientation of the mesopore channels that should lead to sluggish access to the electrode.[101] Since then, several efforts have been carried out to understand the role of pore orientation in molecular transport. It has been demonstrated that both EASA methods that lead to vertical hexagonal pore arrays and EISA-derived 3D interconnected mesopore structures present high accessibility and fast electrode response. However, to date, no systematic comparison between both methods has been undertaken, which should shed light on this matter. In addition, the possibility of hierarchical meso-/microporosity to improve the electrode accessibility is tempting,[29,177] and some results emerge that demonstrate an increased performance attributable to macropores in electrodes,[178] that could be translated to mesoporous organized thin films.

The electrochemical characterization of MTF-modified electrodes permits researchers to understand some general relevant aspects concerning molecular transport along mesopores. First, there is ample evidence that molecule transport, including exclusion or preconcentration phenomena, can be harnessed by controlling the mesopore size and the pore surface or interior. Interactions with the wall and partition phenomena can lead to increased sensitivity and selectivity by excluding interferences and preconcentrating analytes. However, more studies are necessary in order to understand more precisely the ability of pores and surfaces to preconcentrate or exclude particular molecules and to define the relevance of the mesopore structure derived from EISA and EASA in molecular transport and electrode performance. Several aspects linked to confined transport and electrode dynamics remain yet unexplored. Their in-depth study will no doubt provide a better description of the effect of potential gradients created within the pore systems and how they may affect the transport. For example, radial gradients of potential and/or ion concentration could produce local pH effects, and transport mechanisms linked to diffusio-osmosis can intervene.[179] Harnessing these effects opens the gate to MTF electrodes becoming a sound platform for the new fields of iontronics and biomimetic communications.[180,181]

An aspect that requires particular attention toward analytical applications is the electrode performance in realistic matrices. The role of ionic strength is very relevant, and even modest ion concentrations on the order of millimolar, which are typical in biosamples, can "turn off" molecular exclusion. In biological samples, fouling due to proteins (typically, the formation of a protein corona) is also an issue. So far, some promising work

https://doi.org/10.1021/acsomega.3c02013
ACS Omega 2023, 8, 24128−24152

has demonstrated that molecules of interest in the environmental, food, or health fields can be detected in the nanomolar to millimolar range, with reasonable LODs. In these scenarios, functionalization of the external film surface or pore surface with polyelectrolytes could be an alternative to generate optimized perm-selective nanosystems with improved performance. In general, most of the presented work regarding pollutant determinations is performed in low-ionic-strength solutions of the studied molecule, generally in the absence of heavy interferences. This model can be indeed useful for the analysis of natural waters or water quality control, but other fluids (e.g., in the food or oil industries or in biological fluid sensors) present more stringent requirements regarding matrix and interferences, particularly in surface fouling. Therefore, more work devoted to analyzing real analytical matrices should be carried out in order to exploit the real potential of MTF ion sensing and thus achieve realistic figures of merit. Last, but not least, reproducibility of synthetic methods and sensor response repeatability, both in batch-to-batch production and in long-term operation, are relevant aspects that deserve to be studied when considering scaling up to real analytical devices.

A wide field of opportunities has emerged by combining mesopores with biomolecules. The reported pore-blocking strategies that use the selective assembly of aptamers or host–guest complexes are interesting and a growing concept. The high stability and functionality of electroactive enzymes in mesopores[182,183] anticipate that perm-selectivity and signal amplification can be combined, for example using MTF-embedded enzymes whose activity can be modified through the presence or absence of an analyte. Tandem enzymatic systems could also be used to translate one non-electroactive analyte to an electrode signal, imitating natural systems.

The incorporation of responsive modules to MTF-modified electrodes can indeed be a breakthrough, as it will impart the possibility of creating systems adaptable to external solicitations. A wealth of mesoporous responsive systems that stem from the combination of mesopores, nanoparticles, and stimuli-responsive molecules or polymers is available for exploring this concept, which leads to a wealth of different behaviors, from active gating to autonomous and programmable materials that might, one day, take their own decisions.[7,184−186]

AUTHOR INFORMATION

Corresponding Author

Galo J. A. A. Soler-Illia − *Instituto de Nanosistemas, Escuela de Bio y Nanotecnologías, UNSAM-CONICET, 1650 San Martín, Provincia de Buenos Aires, Argentina;* orcid.org/0000-0001-9984-3806; Email: gsoler-illia@unsam.edu.ar

Authors

María L. Scala-Benuzzi − *INTI-Micro y Nanotecnologías, Instituto Nacional de Tecnología Industrial, 1560 San Martín, Buenos Aires, Argentina; Instituto de Nanosistemas, Escuela de Bio y Nanotecnologías, UNSAM-CONICET, 1650 San Martín, Provincia de Buenos Aires, Argentina;* Present Address: (M.L.S.-B.) INQUISAL, Universidad Nacional de San Luis, San Luis, Argentina

Sol N. Fernández − *INTI-Micro y Nanotecnologías, Instituto Nacional de Tecnología Industrial, 1560 San Martín, Buenos Aires, Argentina; Instituto de Nanosistemas, Escuela de Bio y Nanotecnologías, UNSAM-CONICET, 1650 San Martín, Provincia de Buenos Aires, Argentina; Instituto de Calidad Industrial (INCALIN-UNSAM), 1650 San Martín, Provincia de Buenos Aires, Argentina*

Gustavo Giménez − *INTI-Micro y Nanotecnologías, Instituto Nacional de Tecnología Industrial, 1560 San Martín, Buenos Aires, Argentina*

Gabriel Ybarra − *INTI-Micro y Nanotecnologías, Instituto Nacional de Tecnología Industrial, 1560 San Martín, Buenos Aires, Argentina*

Complete contact information is available at: https://pubs.acs.org/10.1021/acsomega.3c02013

Notes

The authors declare no competing financial interest.

ACKNOWLEDGMENTS

The authors gratefully acknowledge the financial support of UNSAM, CONICET, INCALIN-INTI, and the ANPCyT (projects PICT 2017-4651, PICT 2018-04236, and PICT 2020-03130).

REFERENCES

(1) Soler-Illia, G. J. A. A.; Sanchez, C.; Lebeau, B.; Patarin, J. Chemical Strategies To Design Textured Materials: From Microporous and Mesoporous Oxides to Nanonetworks and Hierarchical Structures. *Chem. Rev.* **2002**, *102* (11), 4093−4138.

(2) Soler-Illia, G. J. A. A.; Azzaroni, O. Multifunctional Hybrids by Combining Ordered Mesoporous Materials and Macromolecular Building Blocks. *Chem. Soc. Rev.* **2011**, *40* (2), 1107.

(3) Suib, S. L. A Review of Recent Developments of Mesoporous Materials. *Chem. Rec.* **2017**, *17* (12), 1169−1183.

(4) Wang, J.; Ma, Q.; Wang, Y.; Li, Z.; Li, Z.; Yuan, Q. New Insights into the Structure-Performance Relationships of Mesoporous Materials in Analytical Science. *Chem. Soc. Rev.* **2018**, *47* (23), 8766−8803.

(5) Cashin, V. B.; Eldridge, D. S.; Yu, A.; Zhao, D. Surface Functionalization and Manipulation of Mesoporous Silica Adsorbents for Improved Removal of Pollutants: A Review. *Environ. Sci. (Camb)* **2018**, *4* (2), 110−128.

(6) Innocenzi, P. Mesoporous Ordered Films via Self-Assembly: Trends and Perspectives. *Chem. Sci.* **2022**, *13* (45), 13264−13279.

(7) Alberti, S.; Soler-Illia, G. J. A. A.; Azzaroni, O. Gated Supramolecular Chemistry in Hybrid Mesoporous Silica Nanoarchitectures: Controlled Delivery and Molecular Transport in Response to Chemical, Physical and Biological Stimuli. *Chem. Commun.* **2015**, *51* (28), 6050−6075.

(8) Contreras, C.; Azzaroni, O.; Soler-Illia, G. J. A. A. Use of Confinement Effects in Mesoporous Materials to Build Tailored Nanoarchitectures. In *Comprehensive Nanoscience and Nanotechnology*, Second ed.; Bradshaw, D., Goreham, R., Gregory, D., Kawata, S., Tilley, R., Eds.; Elsevier, 2019; p 10420.

(9) Grosso, D.; Cagnol, F.; Soler-Illia, G. J. D. A. A.; Crepaldi, E. L.; Amenitsch, H.; Brunet-Bruneau, A.; Bourgeois, A.; Sanchez, C. Fundamentals of Mesostructuring through Evaporation-Induced Self-Assembly. *Adv. Funct Mater.* **2004**, *14* (4), 309−322.

(10) Walcarius, A.; Kuhn, A. Ordered Porous Thin Films in Electrochemical Analysis. *TrAC - Trends in Analytical Chemistry* **2008**, *27* (7), 593−603.

(11) Huo, Q.; Margolese, D. I.; Stucky, G. D. Surfactant Control of Phases in the Synthesis of Mesoporous Silica-Based Materials. *Chem. Mater.* **1996**, *8* (5), 1147−1160.

(12) Innocenzi, P.; Malfatti, L. Mesoporous Thin Films: Properties and Applications. *Chem. Soc. Rev.* **2013**, *42* (9), 4198−4216.

(13) Yang, H.; Kuperman, A.; Coombs, N.; Mamiche-Afara, S.; Ozin, G. A. Synthesis of Oriented Films of Mesoporous Silica on Mica. *Nature* **1996**, *379* (6567), 703−705.

(14) Yang, H.; Coombs, N.; Sokolov, I.; Ozin, G. A. Free-Standing and Oriented Mesoporous Silica Films Grown at the Air-Water Interface. *Nature* **1996**, *381* (6583), 589−592.
(15) Brinker, C. J.; Lu, Y.; Sellinger, A.; Fan, H. Evaporation-Induced Self-Assembly: Nanostructures Made Easy. *Adv. Mater.* **1999**, *11* (7), 579−585.
(16) Kim, Y. J.; Lee, Y. H.; Lee, M. H.; Kim, H. J.; Pan, J. H.; Lim, G. Il; Choi, Y. S.; Kim, K.; Park, N.-G.; Lee, C. Formation of Efficient Dye-Sensitized Solar Cells by Introducing an Interfacial Layer of Long-Range Ordered Mesoporous TiO2 Thin Film. *Langmuir* **2008**, *24* (22), 13225−13230.
(17) Hernández-Granados, A.; Corpus-Mendoza, A. N.; Moreno-Romero, P. M.; Rodríguez-Castañeda, C. A.; Pascoe-Sussoni, J. E.; Castelo-González, O. A.; Menchaca-Campos, E. C.; Escorcia-García, J.; Hu, H. Optically Uniform Thin Films of Mesoporous TiO2 for Perovskite Solar Cell Applications. *Opt Mater. (Amst)* **2019**, *88*, 695−703.
(18) Wang, Y.; Guo, J.; Wang, T.; Shao, J.; Wang, D.; Yang, Y.-W. Mesoporous Transition Metal Oxides for Supercapacitors. *Nanomaterials* **2015**, *5* (4), 1667−1689.
(19) Celik, E.; Ma, Y.; Brezesinski, T.; Elm, M. T. Ordered Mesoporous Metal Oxides for Electrochemical Applications: Correlation between Structure, Electrical Properties and Device Performance. *Phys. Chem. Chem. Phys.* **2021**, *23* (18), 10706−10735.
(20) Li, H.; Wu, S.; Hood, Z. D.; Sun, J.; Hu, B.; Liang, C.; Yang, S.; Xu, Y.; Jiang, B. Atomic Defects in Ultra-Thin Mesoporous TiO2 Enhance Photocatalytic Hydrogen Evolution from Water Splitting. *Appl. Surf. Sci.* **2020**, *513*, 145723.
(21) Abdelsamad, A. M. A.; Khalil, A. S. G.; Ulbricht, M. Influence of Controlled Functionalization of Mesoporous Silica Nanoparticles as Tailored Fillers for Thin-Film Nanocomposite Membranes on Desalination Performance. *J. Membr. Sci.* **2018**, *563*, 149−161.
(22) Katsiaounis, S.; Panidi, J.; Koutselas, I.; Topoglidis, E. Fully Reversible Electrically Induced Photochromic-Like Behaviour of Ag:TiO2 Thin Films. *Coatings* **2020**, *10*, 130.
(23) Li, Y.; Li, R.; Bian, H.; Hu, H.; Zhang, K.; Han, P. Photonic Crystal Films with High Reflectance Based on Mesoporous Silica in the Extreme Ultraviolet Range. *Opt. Commun.* **2020**, *474*, 126110.
(24) Kumar, P.; Kim, K.-H.; Vellingiri, K.; Samaddar, P.; Kumar, P.; Deep, A.; Kumar, N. Hybrid Porous Thin Films: Opportunities and Challenges for Sensing Applications. *Biosens Bioelectron* **2018**, *104*, 120−137.
(25) Walcarius, A. Silica-Based Electrochemical Sensors and Biosensors: Recent Trends. *Curr. Opin Electrochem* **2018**, *10*, 88−97.
(26) Etienne, M.; Zhang, L.; Vilà, N.; Walcarius, A. Mesoporous Materials-Based Electrochemical Enzymatic Biosensors. *Electroanalysis* **2015**, *27* (9), 2028−2054.
(27) Sanchez, C.; Boissière, C.; Grosso, D.; Laberty, C.; Nicole, L. Design, Synthesis, and Properties of Inorganic and Hybrid Thin Films Having Periodically Organized Nanoporosity. *Chem. Mater.* **2008**, *20* (3), 682−737.
(28) Soler-Illia, G. J. A. A.; Innocenzi, P. Mesoporous Hybrid Thin Films: The Physics and Chemistry Beneath. *Chem.—Eur. J.* **2006**, *12* (17), 4478−4494.
(29) Innocenzi, P.; Malfatti, L.; Soler-Illia, G. J. A. A. Hierarchical Mesoporous Films: From Self-Assembly to Porosity with Different Length Scales. *Chem. Mater.* **2011**, *23* (10), 2501−2509.
(30) Nasir, T.; Herzog, G.; Hébrant, M.; Despas, C.; Liu, L.; Walcarius, A. Mesoporous Silica Thin Films for Improved Electrochemical Detection of Paraquat. *ACS Sens* **2018**, *3* (2), 484−493.
(31) Giménez, G. Fabricación y Caracterización de Arreglos de Electrodos Recubiertos Con Películas Delgadas Mesoporosas de Óxido de Silicio y Óxidos Mixtos de Silicio y Circonio. Universidad de Buenos Aires, 2018.
(32) Otal, E. H.; Angelomé, P. C.; Bilmes, S. A.; Soler-Illia, G. J. A. A. Functionalized Mesoporous Hybrid Thin Films as Selective Membranes. *Adv. Mater.* **2006**, *18* (7), 934−938.
(33) Fattakhova-Rohlfing, D.; Wark, M.; Rathouský, J. Ion-Permselective PH-Switchable Mesoporous Silica Thin Layers. *Chem. Mater.* **2007**, *19* (7), 1640−1647.
(34) Gaitán, M.; Gonçales, V. R.; Soler-Illia, G. J. A. A.; Baraldo, L. M.; de Torresi, S. I. C. Structure Effects of Self-Assembled Prussian Blue Confined in Highly Organized Mesoporous TiO2 on the Electrocatalytic Properties towards H2O2 Detection. *Biosens Bioelectron* **2010**, *26* (2), 890−893.
(35) Walcarius, A. Mesoporous Materials and Electrochemistry. *Chem. Soc. Rev.* **2013**, *42* (9), 4098−4140.
(36) Tallman, D. E.; Petersen, S. L. Composite Electrodes for Electroanalysis: Principles and Applications. *Electroanalysis* **1990**, *2*, 499−510.
(37) Tashkhourian, J.; Daneshi, M.; Nami-Ana, F.; Behbahani, M.; Bagheri, A. Simultaneous Determination of Hydroquinone and Catechol at Gold Nanoparticles Mesoporous Silica Modified Carbon Paste Electrode. *J. Hazard Mater.* **2016**, *318*, 117−124.
(38) Fang, H. T.; Liu, M.; Wang, D. W.; Sun, T.; Guan, D. S.; Li, F.; Zhou, J.; Sham, T. K.; Cheng, H. M. Comparison of the Rate Capability of Nanostructured Amorphous and Anatase TiO2 for Lithium Insertion Using Anodic TiO2 Nanotube Arrays. *Nanotechnology* **2009**, *20* (22), 225701.
(39) Xiao, H.; Guo, W.; Sun, B.; Pei, M.; Zhou, G. Mesoporous TiO2 and Co-Doped TiO2 Nanotubes/Reduced Graphene Oxide Composites as Electrodes for Supercapacitors. *Electrochim. Acta* **2016**, *190*, 104−117.
(40) Bai, Y.; Yang, H.; Yang, W.; Li, Y.; Sun, C. Gold Nanoparticles-Mesoporous Silica Composite Used as an Enzyme Immobilization Matrix for Amperometric Glucose Biosensor Construction. *Sens Actuators B Chem.* **2007**, *124*, 179−186.
(41) Canevari, T. C.; Raymundo-Pereira, P. A.; Landers, R.; Benvenutti, E. V.; Machado, S. A. S. Sol-Gel Thin-Film Based Mesoporous Silica and Carbon Nanotubes for the Determination of Dopamine, Uric Acid and Paracetamol in Urine. *Talanta* **2013**, *116*, 726−735.
(42) Faustini, M.; Louis, B.; Albouy, P. A.; Kuemmel, M.; Grosso, D. Preparation of Sol-Gel Films by Dip-Coating in Extreme Conditions. *J. Phys. Chem. C* **2010**, *114* (17), 7637−7645.
(43) Faustini, M.; Boissière, C.; Nicole, L.; Grosso, D. From Chemical Solutions to Inorganic Nanostructured Materials: A Journey into Evaporation-Driven Processes. *Chem. Mater.* **2014**, *26* (1), 709−723.
(44) Grosso, D.; Cagnol, F.; Soler-Illia, G. J. A. A.; Crepaldi, E. L.; Amenitsch, H.; Brunet-Bruneau, A.; Bourgeois, A.; Sanchez, C. Fundamentals of Mesostructuring Through Evaporation-Induced Self-Assembly. *Adv. Funct Mater.* **2004**, *14*, 309.
(45) Teng, Z.; Zheng, G.; Dou, Y.; Li, W.; Mou, C. Y.; Zhang, X.; Asiri, A. M.; Zhao, D. Highly Ordered Mesoporous Silica Films with Perpendicular Mesochannels by a Simple Stöber-Solution Growth Approach. *Angewandte Chemie - International Edition* **2012**, *51* (9), 2173−2177.
(46) Walcarius, A.; Sibottier, E.; Etienne, M.; Ghanbaja, J. Electrochemically Assisted Self-Assembly of Mesoporous Silica Thin Films. *Nat. Mater.* **2007**, *6*, 602−608.
(47) Soler-Illia, G. J. A. A.; Innocenzi, P. Mesoporous Hybrid Thin Films: The Physics and Chemistry Beneath. *Chem.—Eur. J.* **2006**, *12*, 4478−4494.
(48) Pai, R. A.; Humayun, R.; Schulberg, M. T.; Sengupta, A.; Sun, J. N.; Watkins, J. J. Mesoporous Silicates Prepared Using Preorganized Templates in Supercritical Fluids. *Science (1979)* **2004**, *303* (5657), 507−510.
(49) Brinker, C. J.; Lu, Y.; Sellinger, A.; Fan, H. Evaporation-Induced Self-Assembly: Functional Nanostructures Made Easy. *Adv. Mater.* **1999**, *11* (7), 579−585.
(50) Huo, Q.; Margolese, D. I.; Stucky, G. D. Surfactant Control of Phases in the Synthesis of Mesoporous Silica-Based Materials. *Chem. Mater.* **1996**, *8* (5), 1147−1160.
(51) Tang, Q.; Angelomé, P. C.; Soler-Illia, G. J. A. A.; Müller, M. Formation of Ordered Mesostructured TiO2 Thin Films: A Soft

https://doi.org/10.1021/acsomega.3c02013
ACS Omega 2023, 8, 24128−24152

Coarse-Grained Simulation Study. *Phys. Chem. Chem. Phys.* **2017**, *19* (41), 28249−28262.
(52) Gazoni, R. M.; Bellino, M. G.; Cecilia Fuertes, M.; Giménez, G.; Soler-Illia, G. J. A. A.; Ricci, M. L. M. Designed Nanoparticle-Mesoporous Multilayer Nanocomposites as Tunable Plasmonic-Photonic Architectures for Electromagnetic Field Enhancement. *J. Mater. Chem. C Mater.* **2017**, *5* (14), 3445−3455.
(53) Giordano, G.; Vilà, N.; Aubert, E.; Ghanbaja, J.; Walcarius, A. Multi-Layered, Vertically-Aligned and Functionalized Mesoporous Silica Films Generated by Sequential Electrochemically Assisted Self-Assembly. *Electrochim. Acta* **2017**, *237*, 227−236.
(54) Vanheusden, G.; Philipsen, H.; Herregods, S. J. F.; Vereecken, P. M. Aggregate-Free Micrometer-Thick Mesoporous Silica Thin Films on Planar and Three-Dimensional Structured Electrodes by Hydrodynamic Diffusion Layer Control during Electrochemically Assisted Self-Assembly. *Chem. Mater.* **2021**, *33* (17), 7075−7088.
(55) Moehl, G. E.; Nasir, T.; Han, Y.; Noori, Y. J.; Huang, R.; Beanland, R.; Bartlett, P. N.; Hector, A. L. AC-Assisted Deposition of Aggregate Free Silica Films with Vertical Pore Structure. *Nanoscale* **2022**, *14* (14), 5404−5411.
(56) Doshi, D. a.; Huesing, N. K.; Lu, M.; Fan, H.; Lu, Y.; Simmons-Potter, K.; Potter, B. G.; Hurd, a J.; Brinker, C. J. Optically Defined Multifunctional Patterning of Photosensitive Thin-Film Silica Mesophases. *Science* **2000**, *290* (5489), 107−111.
(57) Mohamed, N. A. N.; Han, Y.; Hector, A. L.; Houghton, A. R.; Hunter-Sellars, E.; Reid, G.; Williams, D. R.; Zhang, W. Increasing the Diameter of Vertically Aligned, Hexagonally Ordered Pores in Mesoporous Silica Thin Films. *Langmuir* **2022**, *38* (7), 2257−2266.
(58) Soler-Illia, G. J. A. A.; Angelomé, P. C.; Fuertes, M. C.; Grosso, D.; Boissiere, C. Critical Aspects in the Production of Periodically Ordered Mesoporous Titania Thin Films. *Nanoscale* **2012**, *4* (8), 2549−2566.
(59) Fontaine, O.; Laberty-Robert, C.; Sanchez, C. Sol-Gel Route to Zirconia-Pt-Nanoelectrode Arrays 8 Nm in Radius: Their Geometrical Impact in Mass Transport. *Langmuir* **2012**, *28* (7), 3650−3657.
(60) Grosso, D.; Boissière, C.; Smarsly, B.; Brezesinski, T.; Pinna, N.; Albouy, P. A.; Amenitsch, H.; Antonietti, M.; Sanchez, C. Periodically Ordered Nanoscale Islands and Mesoporous Films Composed of Nanocrystalline Multimetallic Oxides. *Nat. Mater.* **2004**, *3* (11), 787−792.
(61) Tang, J.; Wu, Y.; McFarland, E. W.; Stucky, G. D. Synthesis and Photocatalytic Properties of Highly Crystalline and Ordered Mesoporous TiO2 Thin Films. *Chem. Commun.* **2004**, No. 14, 1670−1671.
(62) Pan, J. H.; Lee, W. I. Preparation of Highly Ordered Cubic Mesoporous WO3/TiO2 Films and Their Photocatalytic Properties. *Chem. Mater.* **2006**, *18* (3), 847−853.
(63) Brezesinski, T.; Wang, J.; Tolbert, S. H.; Dunn, B. Ordered Mesoporous α-MoO3 with Iso-Oriented Nanocrystalline Walls for Thin-Film Pseudocapacitors. *Nat. Mater.* **2010**, *9* (2), 146−151.
(64) Brezesinski, K.; Wang, J.; Haetge, J.; Reitz, C.; Steinmueller, S. O.; Tolbert, S. H.; Smarsly, B. M.; Dunn, B.; Brezesinski, T. Pseudocapacitive Contributions to Charge Storage in Highly Ordered Mesoporous Group V Transition Metal Oxides with Iso-Oriented Layered Nanocrystalline Domains. *J. Am. Chem. Soc.* **2010**, *132* (20), 6982−6990.
(65) Feng, D.; Lv, Y.; Wu, Z.; Dou, Y.; Han, L.; Sun, Z.; Xia, Y.; Zheng, G.; Zhao, D. Free-Standing Mesoporous Carbon Thin Films with Highly Ordered Pore Architectures for Nanodevices. *J. Am. Chem. Soc.* **2011**, *133* (38), 15148−15156.
(66) Nishiyama, Y.; Tanaka, S.; Hillhouse, H. W.; Nishiyama, N.; Egashira, Y.; Ueyama, K. Synthesis of Ordered Mesoporous Zirconium Phosphate Films by Spin Coating and Vapor Treatments. *Langmuir* **2006**, *22* (23), 9469−9472.
(67) Andrini, L.; Angelomé, P. C.; Soler-Illia, G. J. A. A.; Requejo, F. G. Understanding the Zr and Si Interdispersion in Zr1-XSixO2Mesoporous Thin Films by Using FTIR and XANES Spectroscopy. *Dalton Transactions* **2016**, *45* (24), 9977−9987.
(68) Innocenzi, P.; Malfatti, L. Mesoporous Thin Films: Properties and Applications. *Chem. Soc. Rev.* **2013**, *42* (9), 4198−4216.
(69) Soler-Illia, G. J. A. A.; Vensaus, P.; Onna, D. Chemical Methods to Produce Mesoporous Thin Films with Tunable Properties. *Chemical Solution Synthesis for Materials Design and Thin Film Device Applications*; Elsevier, 2021; Chapter 6, pp 195−229. .
(70) Etienne, M.; Guillemin, Y.; Grosso, D.; Walcarius, A. Electrochemical Approaches for the Fabrication and/or Characterization of Pure and Hybrid Templated Mesoporous Oxide Thin Films: A Review. *Anal Bioanal Chem.* **2013**, *405* (5), 1497−1512.
(71) Grosso, D.; Cagnol, F.; Soler-Illia, G. J. D. A. A.; Crepaldi, E. L.; Amenitsch, H.; Brunet-Bruneau, A.; Bourgeois, A.; Sanchez, C. Fundamentals of Mesostructuring through Evaporation-Induced Self-Assembly. *Adv. Funct Mater.* **2004**, *14* (4), 309.
(72) Innocenzi, P.; Malfatti, L.; Kidchob, T.; Falcaro, P.; Guidi, M. C.; Piccinini, M.; Marcelli, A. Kinetics of Polycondensation Reactions during Self-Assembly of Mesostructured Films Studied by in Situ Infrared Spectroscopy. *Chem. Commun.* **2005**, No. 18, 2384−2386.
(73) Tang, Q.; Angelomé, P. C.; Soler-Illia, G. J. A. A.; Müller, M. Formation of Ordered Mesostructured TiO2 Thin Films: A Soft Coarse-Grained Simulation Study. *Phys. Chem. Chem. Phys.* **2017**, *19* (41), 28249−28262.
(74) Crepaldi, E. L.; Soler-Illia, G. J. D. A. A.; Grosso, D.; Cagnol, F.; Ribot, F.; Sanchez, C. Controlled Formation of Highly Organized Mesoporous Titania Thin Films: From Mesostructured Hybrids to Mesoporous Nanoanatase TiO_2. *J. Am. Chem. Soc.* **2003**, *125* (32), 9770.
(75) Cagnol, F.; Grosso, D.; Soler-Illia, G. J. D. A. A.; Crepaldi, E. L.; Babonneau, F.; Amenitsch, H.; Sanchez, C. Humidity-Controlled Mesostructuration in CTAB-Templated Silica Thin Film Processing. The Existence of a Modulable Steady State. *J. Mater. Chem.* **2003**, *13* (1), 61.
(76) Mohamed, N. A. N.; Han, Y.; Hector, A. L.; Houghton, A. R.; Hunter-Sellars, E.; Reid, G.; Williams, D. R.; Zhang, W. Increasing the Diameter of Vertically Aligned, Hexagonally Ordered Pores in Mesoporous Silica Thin Films. *Langmuir* **2022**, *38* (7), 2257−2266.
(77) Alvarez-Fernandez, A.; Reid, B.; Fornerod, M. J.; Taylor, A.; Divitini, G.; Guldin, S. Structural Characterization of Mesoporous Thin Film Architectures: A Tutorial Overview. *ACS Appl. Mater. Interfaces* **2020**, *12* (5), 5195−5208.
(78) Lionello, D. F.; Ramallo, J. I.; Soler-Illia, G. J. A. A.; Fuertes, M. C. Mechanical Properties of Ordered Mesoporous Oxides Thin Films. *J. Solgel Sci. Technol.* **2022**, *101* (1), 114−139.
(79) Brinker, C. J.; Scherer, G. W. Sol-Gel Science: The Physics and Chemistry of Sol-Gel Processing. *Sol-Gel Science*; Academic Press, Inc., 1990.
(80) Pierre, A. C. *Introduction to Sol-Gel Processing*; Springer Nature, 2020.
(81) de A. A. Soler-Illia, G. J.; Sanchez, C. Interactions between Poly(Ethylene Oxide)-Based Surfactants and Transition Metal Alkoxides: Their Role in the Templated Construction of Mesostructured Hybrid Organic-Inorganic Composites. *New J. Chem.* **2000**, *24* (7), 493.
(82) Soler-Illia, G. J. A. A.; Angelomé, P. C.; Fuertes, M. C.; Grosso, D.; Boissiere, C. Critical Aspects in the Production of Periodically Ordered Mesoporous Titania Thin Films. *Nanoscale* **2012**, *4* (8), 2549−2566.
(83) Tang, Q.; Angelomé, P. C.; Soler-Illia, G. J. A. A.; Müller, M. Formation of Ordered Mesostructured TiO2 Thin Films: A Soft Coarse-Grained Simulation Study. *Phys. Chem. Chem. Phys.* **2017**, *19* (41), 28249−28262.
(84) Tarutani, N.; Tokudome, Y.; Jobbágy, M.; Soler-Illia, G. J. A. A.; Tang, Q.; Müller, M.; Takahashi, M. Highly Ordered Mesoporous Hydroxide Thin Films through Self-Assembly of Size-Tailored Nanobuilding Blocks: A Theoretical-Experimental Approach. *Chem. Mater.* **2019**, *31* (2), 322−330.
(85) Weidmann, C.; Brezesinski, K.; Suchomski, C.; Tropp, K.; Grosser, N.; Haetge, J.; Smarsly, B. M.; Brezesinski, T. Morphology-Controlled Synthesis of Nanocrystalline η-Al2O3 Thin Films,

https://doi.org/10.1021/acsomega.3c02013
ACS Omega 2023, 8, 24128−24152

Powders, Microbeads, and Nanofibers with Tunable Pore Sizes from Preformed Oligomeric Oxo-Hydroxo Building Blocks. *Chem. Mater.* **2012**, *24* (3), 486−494.
(86) Hong, M.-H.; Choi, H.; Kim, Y.; Shim, D. Il; Cho, H. H.; Park, H.-H. Thermoelectric Behaviors of ZnO Mesoporous Thin Films Affected by Strain Induced from the Different Dopants Radii (Al, Ga, and In). *Appl. Phys. Lett.* **2021**, *119* (19), 193902.
(87) Hong, M.-H.; Choi, H.; Kim, Y.; Kim, T.; Cho, H. H.; Driss, Z.; Driss, D.; Bouabidi, A.; Euchy, S.; Park, H.-H. Ti Doping Effects on the Seebeck Coefficient and Electrical Conductivity of Mesoporous ZnO Thin Film. *Mater. Chem. Phys.* **2019**, *235*, 121757.
(88) Tarutani, N.; Tokudome, Y.; Jobbágy, M.; Viva, F. A.; Soler-Illia, G. J. A. A.; Takahashi, M. Single-Nanometer-Sized Low-Valence Metal Hydroxide Crystals: Synthesis via Epoxide-Mediated Alkalinization and Assembly toward Functional Mesoporous Materials. *Chem. Mater.* **2016**, *28* (16), 5606−5610.
(89) Tarutani, N.; Tokudome, Y.; Jobbágy, M.; Soler-Illia, G. J. A. A.; Tang, Q.; Müller, M.; Takahashi, M. Highly Ordered Mesoporous Hydroxide Thin Films through Self-Assembly of Size-Tailored Nanobuilding Blocks: A Theoretical-Experimental Approach. *Chem. Mater.* **2019**, *31* (2), 322.
(90) Yang, P.; Zhao, D.; Margolese, D. I.; Chmelka, B. F.; Stucky, G. D. Block Copolymer Templating Syntheses of Mesoporous Metal Oxides with Large Ordering Lengths and Semicrystalline Framework. *Chem. Mater.* **1999**, *11* (10), 2813−2826.
(91) Calvo, A.; Angelomé, P. C.; Sánchez, V. M.; Scherlis, D. A.; Williams, F. J.; Soler-Illia, G. J. A. A. Mesoporous Aminopropyl-Functionalized Hybrid Thin Films with Modulable Surface and Environment-Responsive Behavior. *Chem. Mater.* **2008**, *20* (14), 4661−4668.
(92) Nishiyama, N.; Tanaka, S.; Egashira, Y.; Oku, Y.; Ueyama, K. Enhancement of Structural Stability of Mesoporous Silica Thin Films Prepared by Spin-Coating. *Chem. Mater.* **2002**, *14* (10), 4229−4234.
(93) Violi, I. L.; Perez, M. D.; Fuertes, M. C.; Soler-Illia, G. J. A. A. Highly Ordered, Accessible and Nanocrystalline Mesoporous TiO 2 Thin Films on Transparent Conductive Substrates. *ACS Appl. Mater. Interfaces* **2012**, *4* (8), 4320−4330.
(94) Crepaldi, E. L.; Soler-Illia, G. J. de A. A.; Grosso, D.; Sanchez, C. Nanocrystallised Titania and Zirconia Mesoporous Thin Films Exhibiting Enhanced Thermal Stability. *New J. Chem.* **2003**, *27* (1), 9−13.
(95) Grosso, D.; Soler-Illia, G. J. D. A. A.; Crepaldi, E. L.; Cagnol, F.; Sinturel, C.; Bourgeois, A.; Brunet-Bruneau, A.; Amenitsch, H.; Albouy, P. A.; Sanchez, C. Highly Porous TiO_2 Anatase Optical Thin Films with Cubic Mesostructure Stabilized at 700 °C. *Chem. Mater.* **2003**, *15* (24), 4562.
(96) Angelomé, P. C.; Andrini, L.; Calvo, M. E.; Requejo, F. G.; Bilmes, S. A.; Soler-Illia, G. J. A. A. Mesoporous Anatase TiO2 Films: Use of Ti K XANES for the Quantification of the Nanocrystalline Character and Substrate Effects in the Photocatalysis Behavior. *J. Phys. Chem. C* **2007**, *111* (29), 10886−10893.
(97) Jara Fornerod, M. J.; Alvarez-Fernandez, A.; Williams, E. R.; Skoda, M. W. A.; Prieto-Simon, B.; Voelcker, N. H.; Stefik, M.; Coppens, M.-O.; Guldin, S. Enhanced Structural Control of Soft-Templated Mesoporous Inorganic Thin Films by Inert Processing Conditions. *ACS Appl. Mater. Interfaces* **2022**, *14* (50), 56143−56155.
(98) Giménez, G.; Ybarra, G.; Soler-Illia, G. J. A. A. Preparation of Mesoporous Silica Thin Films at Low Temperature: A Comparison of Mild Structure Consolidation and Template Extraction Procedures. *J. Solgel Sci. Technol.* **2020**, *96* (2), 287−296.
(99) Joó, P. Porosity and Permeability of Clay Films: An Electrochemical Survey. In *From Colloids to Nanotechnology*; Progress in Colloid and Polymer Science; Zrínyi, M., Hórvölgyi, Z. D., Eds.; Springer Berlin Heidelberg: Berlin, Heidelberg, 2004; Vol. 125, pp 74−79.
(100) Zürner, A.; Kirstein, J.; Döblinger, M.; Bräuchle, C.; Bein, T. Visualizing Single-Molecule Diffusion in Mesoporous Materials. *Nature* **2007**, *450* (7170), 705−708.
(101) Song, C.; Villemure, G. Electrode Modification with Spin-Coated Films of Mesoporous Molecular Sieve Silicas. *Microporous Mesoporous Mater.* **2001**, *44*−*45*, 679−689.
(102) Zhuravlev, L. T. The Surface Chemistry of Amorphous Silica. Zhuravlev Model. *Colloids Surf. A Physicochem Eng. Asp* **2000**, *173* (1−3), 1−38.
(103) Wu, S. H.; Lin, H. P. Synthesis of Mesoporous Silica Nanoparticles. *Chem. Soc. Rev.* **2013**, *42* (9), 3862−3875.
(104) Allouni, Z. E.; Cimpan, M. R.; Høl, P. J.; Skodvin, T.; Gjerdet, N. R. Agglomeration and Sedimentation of TiO2 Nanoparticles in Cell Culture Medium. *Colloids Surf. B Biointerfaces* **2009**, *68* (1), 83−87.
(105) Kosmulski, M. PH-Dependent Surface Charging and Points of Zero Charge. IV. Update and New Approach. *J. Colloid Interface Sci.* **2009**, *337* (2), 439−448.
(106) Bard, A. J.; Faulkner, L. R. *Electrochemical Methods: Fundamentals and Applications*, 2nd ed.; John Wiley and Sons: New York, 2001.
(107) Angiolini, J. F.; Stortz, M.; Steinberg, P. Y.; Mocskos, E.; Bruno, L.; Soler-Illia, G.; Angelomé, P. C.; Wolosiuk, A.; Levi, V. Diffusion of Single Dye Molecules in Hydrated TiO2Mesoporous Films. *Phys. Chem. Chem. Phys.* **2017**, *19* (39), 26540−26544.
(108) Andrieu-Brunsen, A.; Micoureau, S.; Tagliazucchi, M.; Szleifer, I.; Azzaroni, O.; Soler-Illia, G. J. A. A. Mesoporous Hybrid Thin Film Membranes with PMETAC@Silica Architectures: Controlling Ionic Gating through the Tuning of Polyelectrolyte Density. *Chem. Mater.* **2015**, *27* (3), 808−821.
(109) Fattakhova-Rohlfing, D.; Wark, M.; Rathouský, J. Ion-Permselective PH-Switchable Mesoporous Silica Thin Layers. *Chem. Mater.* **2007**, *19* (7), 1640−1647.
(110) Brunsen, A.; Calvo, A.; Williams, F. J.; Soler-Illia, G. J. A. A.; Azzaroni, O. Manipulation of Molecular Transport into Mesoporous Silica Thin Films by the Infiltration of Polyelectrolytes. *Langmuir* **2011**, *27* (8), 4328−4333.
(111) Calvo, A.; Yameen, B.; Williams, F. J.; Soler-Illia, G. J. A. A.; Azzaroni, O. Mesoporous Films and Polymer Brushes Helping Each Other to Modulate Ionic Transport in Nanoconfined Environments. An Interesting Example of Synergism in Functional Hybrid Assemblies. *J. Am. Chem. Soc.* **2009**, *131* (31), 10866−10868.
(112) Steinberg, P. Y.; Zanotto, F. M.; Soler-Illia, G. J. A. A.; Dassie, S. A.; Angelomé, P. C. Molecular Transport through TiO_2 Mesoporous Thin Films: Correlation with the Partially Blocked Electrode Model. *J. Phys. Chem. C* **2021**, *125* (42), 23521−23532.
(113) Giménez, G. Fabricación y caracterización de arreglos de electrodos recubiertos con películas delgadas mesoporosas de óxido de silicio y óxidos mixtos de silicio y circonio. Tesis Doctoral, Universidad de Buenos Aires. Facultad de Ciencias Exactas y Naturales, 2018 (https://hdl.handle.net/20.500.12110/tesis_n6373_Gimenez).
(114) Alberti, S.; Steinberg, P. Y.; Giménez, G.; Amenitsch, H.; Ybarra, G.; Azzaroni, O.; Angelomé, P. C.; Soler-Illia, G. J. A. A. Chemical Stability of Mesoporous Oxide Thin Film Electrodes under Electrochemical Cycling: From Dissolution to Stabilization. *Langmuir* **2019**, *35* (19), 6279−6287.
(115) Nasir, T.; Vodolazkaya, N. A.; Herzog, G.; Walcarius, A. Critical Effect of Film Thickness on Preconcentration Electroanalysis with Oriented Mesoporous Silica Modified Electrodes. *Electroanalysis* **2019**, *31* (2), 202−207.
(116) Etienne, M.; Quach, A.; Grosso, D.; Nicole, L.; Sanchez, C.; Walcarius, A. Molecular Transport into Mesostructured Silica Thin Films: Electrochemical Monitoring and Comparison between P6m, $P63/Mmc$, and $Pm3n$ Structures. *Chem. Mater.* **2007**, *19* (4), 844−856.
(117) Karman, C.; Vilà, N.; Walcarius, A. Amplified Charge Transfer for Anionic Redox Probes through Oriented Mesoporous Silica Thin Films. *ChemElectroChem.* **2016**, *3* (12), 2130−2137.
(118) Goux, A.; Etienne, M.; Aubert, E.; Lecomte, C.; Ghanbaja, J.; Walcarius, A. Oriented Mesoporous Silica Films Obtained by Electro-Assisted Self-Assembly (EASA). *Chem. Mater.* **2009**, *21* (4), 731−741.

https://doi.org/10.1021/acsomega.3c02013
ACS Omega 2023, 8, 24128−24152

(119) Wang, J.; Vilà, N.; Walcarius, A. Redox-Active Vertically Aligned Mesoporous Silica Thin Films as Transparent Surfaces for Energy Storage Applications. *ACS Appl. Mater. Interfaces* **2020**, *12* (21), 24262−24270.
(120) Nasir, T.; Zhang, L.; Vilà, N.; Herzog, G.; Walcarius, A. Electrografting of 3-Aminopropyltriethoxysilane on a Glassy Carbon Electrode for the Improved Adhesion of Vertically Oriented Mesoporous Silica Thin Films. *Langmuir* **2016**, *32* (17), 4323.
(121) Basnig, D.; Vilá, N.; Herzog, G.; Walcarius, A. Voltammetric Behaviour of Cationic Redox Probes at Mesoporous Silica Film Electrodes. *J. Electroanal. Chem.* **2020**, *872* (xxxx), 113993.
(122) Taffa, D. H.; Kathiresan, M.; Walder, L.; Seelandt, B.; Wark, M. Pore Size and Surface Charge Control in Mesoporous TiO(2) Using Post-Grafted SAMs. *Phys. Chem. Chem. Phys.* **2010**, *12* (7), 1473−1482.
(123) Calvo, A.; Fuertes, M. C.; Yameen, B.; Williams, F. J.; Azzaroni, O.; Soler-Illia, G. J. a a. Nanochemistry in Confined Environments: Polyelectrolyte Brush-Assisted Synthesis of Gold Nanoparticles inside Ordered Mesoporous Thin Films. *Langmuir* **2010**, *26* (8), 5559−5567.
(124) DiMarco, B. N.; Motley, T. C.; Balok, R. S.; Li, G.; Siegler, M. A.; O'Donnell, R. M.; Hu, K.; Meyer, G. J. A Distance Dependence to Lateral Self-Exchange across Nanocrystalline TiO2. A Comparative Study of Three Homologous RuIII/II Polypyridyl Compounds. *J. Phys. Chem. C* **2016**, *120* (26), 14226−14235.
(125) Lee, D.; Jin, Y.; Jung, N.; Lee, J.; Lee, J.; Jeong, Y. S.; Jeon, S. Gravimetric Analysis of the Adsorption and Desorption of CO2 on Amine-Functionalized Mesoporous Silica Mounted on a Microcantilever Array. *Environ. Sci. Technol.* **2011**, *45* (13), 5704−5709.
(126) Wang, R.; Lan, K.; Chen, Z.; Zhang, X.; Hung, C. Te; Zhang, W.; Wang, C.; Wang, S.; Chen, A.; Li, W.; Xu, X.; Zhao, D. Janus Mesoporous Sensor Devices for Simultaneous Multivariable Gases Detection. *Matter* **2019**, *1* (5), 1274−1284.
(127) Argoubi, W.; Sánchez, A.; Parrado, C.; Raouafi, N.; Villalonga, R. Label-Free Electrochemical Aptasensing Platform Based on Mesoporous Silica Thin Film for the Detection of Prostate Specific Antigen. *Sens Actuators B Chem.* **2018**, *255*, 309−315.
(128) Gueshi, T.; Tokuda, K.; Matsuda, H. Voltammetry at Partially Covered Electrodes: Part II. Linear Potential Sweep and Cyclic Voltammetry. *J. Electroanal Chem. Interfacial Electrochem* **1979**, *101* (1), 29−38.
(129) Kisler, J. M.; Dähler, A.; Stevens, G. W.; O'Connor, A. J. Separation of Biological Molecules Using Mesoporous Molecular Sieves. *Microporous Mesoporous Mater.* **2001**, *44*−*45*, 769−774.
(130) López-Puente, V.; Angelomé, P. C.; Soler-Illia, G. J. A. A.; Liz-Marzán, L. M. Selective SERS Sensing Modulated by Functionalized Mesoporous Films. *ACS Appl. Mater. Interfaces* **2015**, *7* (46), 25633.
(131) Serrano, M. B.; Despas, C.; Herzog, G.; Walcarius, A. Mesoporous Silica Thin Films for Molecular Sieving and Electrode Surface Protection against Biofouling. *Electrochem commun* **2015**, *52*, 34−36.
(132) Ghazzal, M. N.; Joseph, M.; Kebaili, H.; De Coninck, J.; Gaigneaux, E. M. Tuning the Selectivity and Sensitivity of Mesoporous Dielectric Multilayers by Modifiying the Hydrophobic-Hydrophilic Balance of the Silica Layer. *J. Mater. Chem.* **2012**, *22* (42), 22526−22532.
(133) Yan, F.; He, Y.; Ding, L.; Su, B. Highly Ordered Binary Assembly of Silica Mesochannels and Surfactant Micelles for Extraction and Electrochemical Analysis of Trace Nitroaromatic Explosives and Pesticides. *Anal. Chem.* **2015**, *87* (8), 4436−4441.
(134) Taffa, D. H.; Kathiresan, M.; Walder, L.; Seelandt, B.; Wark, M. Pore Size and Surface Charge Control in Mesoporous TiO2 Using Post-Grafted SAMs. *Phys. Chem. Chem. Phys.* **2010**, *12* (7), 1473−1482.
(135) Jiokeng, S. L. Z.; Tonle, I. K.; Walcarius, A. Amino-Attapulgite/Mesoporous Silica Composite Films Generated by Electro-Assisted Self-Assembly for the Voltammetric Determination of Diclofenac. *Sens Actuators B Chem.* **2019**, *287*, 296−305.
(136) Yan, F.; Ma, X.; Jin, Q.; Tong, Y.; Tang, H.; Lin, X.; Liu, J. Phenylboronic Acid-Functionalized Vertically Ordered Mesoporous Silica Films for Selective Electrochemical Determination of Fluoride Ion in Tap Water. *Microchimica Acta* **2020**, *187* (8), 470 DOI: 10.1007/s00604-020-04422-4.
(137) Karman, C.; Vilà, N.; Walcarius, A. Amplified Charge Transfer for Anionic Redox Probes through Oriented Mesoporous Silica Thin Films. *ChemElectroChem.* **2016**, *3* (12), 2130−2137.
(138) Vilà, N.; de Oliveira, P.; Walcarius, A.; Mbomekallé, I. M. Permeability of Dawson-Type Polyoxometalates through Vertically Oriented Nanoporous Silica Membranes on Electrode: Effect of Pore Size and Probe Charge. *Electrochim. Acta* **2020**, *353*, 136577.
(139) Taffa, D.; Kathiresan, M.; Walder, L. Tuning the Hydrophilic, Hydrophobic, and Ion Exchange Properties of Mesoporous TiO2. *Langmuir* **2009**, *25* (9), 5371−5379.
(140) Yan, F.; Zheng, W.; Yao, L.; Su, B. Direct Electrochemical Analysis in Complex Samples Using ITO Electrodes Modified with Permselective Membranes Consisting of Vertically Ordered Silica Mesochannels and Micelles. *Chem. Commun.* **2015**, *51* (100), 17736−17739.
(141) Hsu, S. C.; Cheng, H. T.; Wu, P. X.; Weng, C. J.; Santiago, K. S.; Yeh, J. M. Electrochemical Sensor Constructed Using a Carbon Paste Electrode Modified with Mesoporous Silica Encapsulating PANI Chains Decorated with GNPs for Detection of Ascorbic Acid. *Electrochim. Acta* **2017**, *238*, 246−256.
(142) Ahoulou, S.; Vilà, N.; Pillet, S.; Schaniel, D.; Walcarius, A. Non-Covalent Immobilization of Iron-Triazole (Fe(Htrz)3) Molecular Mediator in Mesoporous Silica Films for the Electrochemical Detection of Hydrogen Peroxide. *Electroanalysis* **2020**, *32* (4), 690−697.
(143) Sacara, A. M.; Pitzalis, F.; Salis, A.; Turdean, G. L.; Muresan, L. M. Glassy Carbon Electrodes Modified with Ordered Mesoporous Silica for the Electrochemical Detection of Cadmium Ions. *ACS Omega* **2019**, *4* (1), 1410−1415.
(144) Li, W.; Ding, L.; Wang, Q.; Su, B. Differential Pulse Voltammetry Detection of Dopamine and Ascorbic Acid by Permselective Silica Mesochannels Vertically Attached to the Electrode Surface. *Analyst* **2014**, *139* (16), 3926−3931.
(145) He, Y.; Ding, L.; Su, B. Vertically Ordered Silica Mesochannels as Preconcentration Materials for the Electrochemical Detection of Methylene Blue. *Sci. China Chem.* **2015**, *58* (10), 1593−1599.
(146) Maheshwari, H.; Vilà, N.; Herzog, G.; Walcarius, A. Selective Detection of Cysteine at a Mesoporous Silica Film Electrode Functionalized with Ferrocene in the Presence of Glutathione. *ChemElectroChem.* **2020**, *7* (9), 2095−2101.
(147) Yan, F.; Chen, J.; Jin, Q.; Zhou, H.; Sailjoi, A.; Liu, J.; Tang, W. Fast One-Step Fabrication of a Vertically-Ordered Mesoporous Silica-Nanochannel Film on Graphene for Direct and Sensitive Detection of Doxorubicin in Human Whole Blood. *J. Mater. Chem. C Mater.* **2020**, *8* (21), 7113−7119.
(148) Bass, J. D.; Grosso, D.; Boissiere, C.; Belamie, E.; Coradin, T.; Sanchez, C. Stability of Mesoporous Oxide and Mixed Metal Oxide Materials under Biologically Relevant Conditions. *Chem. Mater.* **2007**, *19* (17), 4349−4356.
(149) Li, W.; Ding, L.; Wang, Q.; Su, B. Differential Pulse Voltammetry Detection of Dopamine and Ascorbic Acid by Permselective Silica Mesochannels Vertically Attached to the Electrode Surface. *Analyst* **2014**, *139* (16), 3926−3931.
(150) Yan, F.; Chen, J.; Jin, Q.; Zhou, H.; Sailjoi, A.; Liu, J.; Tang, W. Fast One-Step Fabrication of a Vertically-Ordered Mesoporous Silica-Nanochannel Film on Graphene for Direct and Sensitive Detection of Doxorubicin in Human Whole Blood. *J. Mater. Chem. C Mater.* **2020**, *8* (21), 7113−7119.
(151) Maheshwari, H.; Vilà, N.; Herzog, G.; Walcarius, A. Selective Detection of Cysteine at a Mesoporous Silica Film Electrode Functionalized with Ferrocene in the Presence of Glutathione. *ChemElectroChem.* **2020**, *7* (9), 2095−2101.

https://doi.org/10.1021/acsomega.3c02013
ACS Omega 2023, 8, 24128−24152

(152) Zhang, A.; Lieber, C. M. Nano-Bioelectronics. *Chem. Rev.* **2016**, *116* (1), 215−257.
(153) Goldsmith, B. R.; Locascio, L.; Gao, Y.; Lerner, M.; Walker, A.; Lerner, J.; Kyaw, J.; Shue, A.; Afsahi, S.; Pan, D.; Nokes, J.; Barron, F. Digital Biosensing by Foundry-Fabricated Graphene Sensors. *Sci. Rep* **2019**, *9* (1), 434.
(154) Angelomé, P. C.; Soler-Illia, G. J. D. A. A. Organically Modified Transition-Metal Oxide Mesoporous Thin Films and Xerogels. *Chem. Mater.* **2005**, *17* (2), 322−331.
(155) Yang, X.; Qiu, P.; Yang, J.; Fan, Y.; Wang, L.; Jiang, W. Mesoporous Materials - Based Electrochemical Biosensors from Enzymatic to Nonenzymatic. *Small* **2021**, *17* (9), 1904022.
(156) Gaitán, M.; Gonçales, V. R.; Soler-Illia, G. J. A. A.; Baraldo, L. M.; de Torresi, S. I. C. Structure Effects of Self-Assembled Prussian Blue Confined in Highly Organized Mesoporous TiO2 on the Electrocatalytic Properties towards H2O2 Detection. *Biosens Bioelectron* **2010**, *26* (2), 890−893.
(157) Saint-André, S.; Albanese, F.; Soler-Illia, G. J. A. A.; Tagliazucchi, M. Charge Percolation in Redox-Active Thin Membrane Hybrids of Mesoporous Silica and Poly (Viologens). *Phys. Chem. Chem. Phys.* **2019**, *21* (5), 2743−2754.
(158) Bellino, M. G.; Soler-Illia, G. J. A. A. Nano-Designed Enzyme-Functionalized Hierarchical Metal-Oxide Mesoporous Thin Films: En Route to Versatile Biofuel Cells. *small* **2014**, *10* (14), 2834−2839.
(159) Bellino, M. G.; Municoy, S.; Soler-Illia, G. J. A. A. Enzymatic Tandem Systems Engineered from Mesoporous Thin Films: Synergy Leading to Efficient Starch-Electricity Conversion. *Mater. Today Commun.* **2016**, *7*, 67−72.
(160) Regiart, M.; Fernández, O.; Vicario, A.; Villarroel-rocha, J.; Sapag, K.; Messina, G. A.; Raba, J.; Bertolino, F. A. Mesoporous Immunosensor Applied to Zearalenone Determination in Amaranthus Cruentus Seeds. *Microchemical Journal* **2018**, *141* (March), 388−394.
(161) Schmidt, S.; Alberti, S.; Vana, P.; Soler-Illia, G. J. A. A.; Azzaroni, O. Thermosensitive Cation-Selective Mesochannels: PNIPAM-Capped Mesoporous Thin Films as Bioinspired Interfacial Architectures with Concerted Functions. *Chem.—Eur. J.* **2017**, *23* (58), 14500−14506.
(162) Zhou, P.; Yao, L.; Chen, K.; Su, B. Silica Nanochannel Membranes for Electrochemical Analysis and Molecular Sieving: A Comprehensive Review. *Crit Rev. Anal Chem.* **2020**, *50* (5), 424−444.
(163) Lee, I.; Kim, S. E.; Lee, J.; Woo, D. H.; Lee, S.; Pyo, H.; Song, C. S.; Lee, J. A Self-Calibrating Electrochemical Aptasensing Platform: Correcting External Interference Errors for the Reliable and Stable Detection of Avian Influenza Viruses. *Biosens. Bioelectron.* **2020**, *152*, 112010.
(164) Duan, W.; Zhi, H.; Keefe, D. W.; Gao, B.; LeFevre, G. H.; Toor, F. Sensitive and Specific Detection of Estrogens Featuring Doped Silicon Nanowire Arrays. *ACS Omega* **2022**, *7* (50), 47341−47348.
(165) Parihar, A.; Choudhary, N. K.; Sharma, P.; Khan, R. Carbon Nanomaterials-Based Electrochemical Aptasensor for Point-of-Care Diagnostics of Cancer Biomarkers. *Mater. Today Chem.* **2023**, *30*, 101499.
(166) Alberti, S.; Piccinini, E.; Ramirez, P. G.; Longo, G. S.; Ceolín, M.; Azzaroni, O. Mesoporous Thin Films on Graphene FETs: Nanofiltered, Amplified and Extended Field-Effect Sensing. *Nanoscale* **2021**, *13* (45), 19098−19108.
(167) Wang, H.; Xiu, Y.; Chen, Y.; Sun, L.; Yang, L.; Chen, H. Electrochemical immunosensor based on an antibody-hierarchical mesoporous SiO_2 for the detection of *Staphylococcus aureus*. *RSC Adv.* **2019**, *9*, 16278−16287.
(168) Cortina, M. E.; Melli, L. J.; Roberti, M.; Mass, M.; Longinotti, G.; Tropea, S.; Lloret, P.; Serantes, D. A. R.; Salomón, F.; Lloret, M.; Caillava, A. J.; Restuccia, S.; Altcheh, J.; Buscaglia, C. A.; Malatto, L.; Ugalde, J. E.; Fraigi, L.; Moina, C.; Ybarra, G.; Ciocchini, A. E.; Comerci, D. J. Electrochemical Magnetic Microbeads-Based Biosensor for Point-of-Care Serodiagnosis of Infectious Diseases. *Biosens Bioelectron* **2016**, *80*, 24−33.
(169) Ainla, A.; Mousavi, M. P. S.; Tsaloglou, M. N.; Redston, J.; Bell, J. G.; Fernández-Abedul, M. T.; Whitesides, G. M. Open-Source Potentiostat for Wireless Electrochemical Detection with Smartphones. *Anal. Chem.* **2018**, *90* (10), 6240−6246.
(170) Agis, L.; Torres, F.; Gak, J.; Miguez, M. Integrated Potentiostat for Detection of Chagas Disease. *International Journal of Circuit Theory and Applications* **2018**, *46* (12), 2299−2313.
(171) Levine, P. M.; Gong, P.; Levicky, R.; Shepard, K. L. Real-Time, Multiplexed Electrochemical DNA Detection Using an Active Complementary Metal-Oxide-Semiconductor Biosensor Array with Integrated Sensor Electronics. *Biosens Bioelectron* **2009**, *24* (7), 1995−2001.
(172) Giagkoulovits, C.; Cheah, B. C.; Al-Rawhani, M. A.; Accarino, C.; Busche, C.; Grant, J. P.; Cumming, D. R. S. A 16 × 16 CMOS Amperometric Microelectrode Array for Simultaneous Electrochemical Measurements. *IEEE Transactions on Circuits and Systems I: Regular Papers* **2018**, *65* (9), 2821−2831.
(173) Arya, S. K.; Wong, C. C.; Jeon, Y. J.; Bansal, T.; Park, M. K. Advances in Complementary-Metal-Oxide-Semiconductor-Based Integrated Biosensor Arrays. *Chem. Rev.* **2015**, *115* (11), 5116−5158.
(174) Lim, B.; Futagawa, M.; Takahashi, S.; Dasai, F.; Ishida, M.; Sawada, K. Integrated 8 × 8 Array Redox Sensor System Employing On-Chip Square Wave Voltammetric Circuit for Multi Point and High-Speed Detection. *Jpn. J. Appl. Phys.* **2014**, *53* (4), 046502.
(175) Rothe, J.; Frey, O.; Stettler, A.; Chen, Y.; Hierlemann, A. Fully Integrated CMOS Microsystem for Electrochemical Measurements on 32 × 32 Working Electrodes at 90 Frames per Second. *Anal. Chem.* **2014**, *86* (13), 6425−6432.
(176) Moya, A.; Pol, R.; Martínez-Cuadrado, A.; Villa, R.; Gabriel, G.; Baeza, M. Stable Full Inkjet-Printed Solid-State Ag/AgCl Reference Electrode. *Anal. Chem.* **2019**, *91*, 15539.
(177) Schneider, D.; Mehlhorn, D.; Zeigermann, P.; Kärger, J.; Valiullin, R. Transport Properties of Hierarchical Micro-Mesoporous Materials. *Chem. Soc. Rev.* **2016**, *45* (12), 3439−3467.
(178) Wang, S.; Guo, P.; Ma, G.; Wei, J.; Wang, Z.; Cui, L.; Sun, L.; Wang, A. Three-Dimensional Hierarchical Mesoporous Carbon for Regenerative Electrochemical Dopamine Sensor. *Electrochim. Acta* **2020**, *360*, 137016.
(179) Shim, S. Diffusiophoresis, Diffusioosmosis, and Microfluidics: Surface-Flow-Driven Phenomena in the Presence of Flow. *Chem. Rev.* **2022**, *122* (7), 6986−7009.
(180) Han, S. H.; Oh, M.-A.; Chung, T. D. Iontronics: Aqueous Ion-Based Engineering for Bioinspired Functionalities and Applications. *Chemical Physics Reviews* **2022**, *3* (3), 031302.
(181) Pizarro, A. D.; Berli, C. L. A.; Soler-Illia, G. J. A. A.; Bellino, M. G. Droplets in Underlying Chemical Communication Recreate Cell Interaction Behaviors. *Nat. Commun.* **2022**, *13* (1), 3047.
(182) Bellino, M. G.; Soler-Illia, G. J. A. A. Nano-Designed Enzyme-Functionalized Hierarchical Metal-Oxide Mesoporous Thin Films: En Route to Versatile Biofuel Cells. *Small* **2014**, *10* (14), 2834.
(183) Bellino, M. G.; Municoy, S.; Soler-Illia, G. J. A. A. Enzymatic Tandem Systems Engineered from Mesoporous Thin Films: Synergy Leading to Efficient Starch-Electricity Conversion. *Mater. Today Commun.* **2016**, *7*, 67−72.
(184) Chen, W.; Cheng, C. A.; Xiang, D.; Zink, J. I. Expanding Nanoparticle Multifunctionality: Size-Selected Cargo Release and Multiple Logic Operations. *Nanoscale* **2021**, *13* (10), 5497−5506.
(185) Tom, J. C.; Appel, C.; Andrieu-Brunsen, A. Fabrication and *in Situ* Functionalisation of Mesoporous Silica Films by the Physical Entrapment of Functional and Responsive Block Copolymer Structuring Agents. *Soft Matter* **2019**, *15* (40), 8077−8083.
(186) García-Fernández, A.; Lozano-Torres, B.; Blandez, J. F.; Monreal-Trigo, J.; Soto, J.; Collazos-Castro, J. E.; Alcañiz, M.; Marcos, M. D.; Sancenón, F.; Martínez-Máñez, R. Electro-Responsive Films Containing Voltage Responsive Gated Mesoporous Silica Nanoparticles Grafted onto PEDOT-Based Conducting Polymer. *J. Controlled Release* **2020**, *323*, 421−430.

https://doi.org/10.1021/acsomega.3c02013
ACS Omega 2023, 8, 24128−24152